AD-A044 021 SYRACUSE UNIV N Y DEPT OF ELECTRICAL AND COMPUTER E--ETC F/G 9/5
TWO-DIMENSIONAL DIRECT ELECTRONIC FOURIER TRANSFORM (DEFT) DEVI--ETC(U)
JUN 77 S T KOWEL, P G KORNREICH, K W LOH DAAG53-76-C-0162
UNCLASSIFIED TR-77-5 NL

1 OF 2
AD
A044021

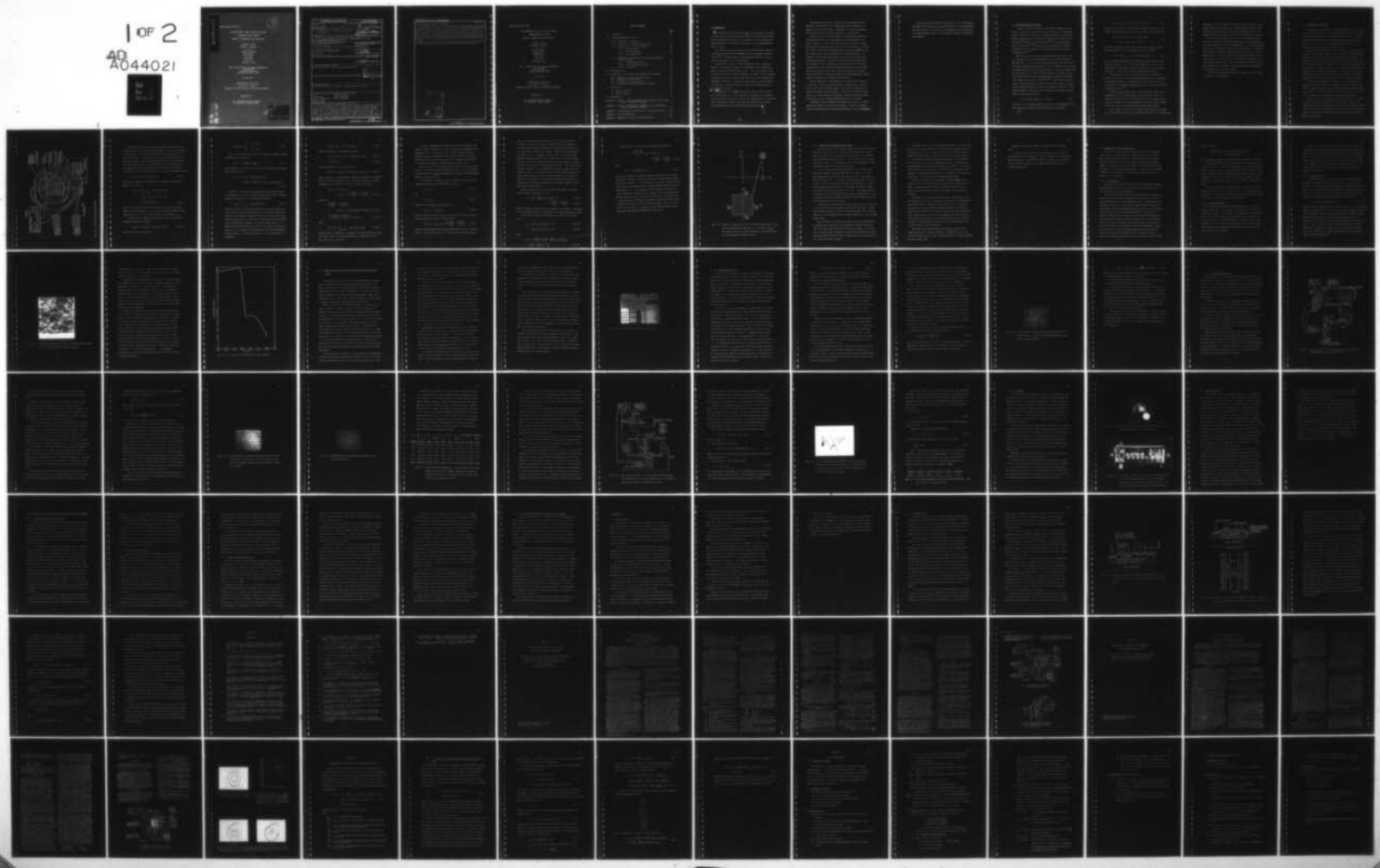

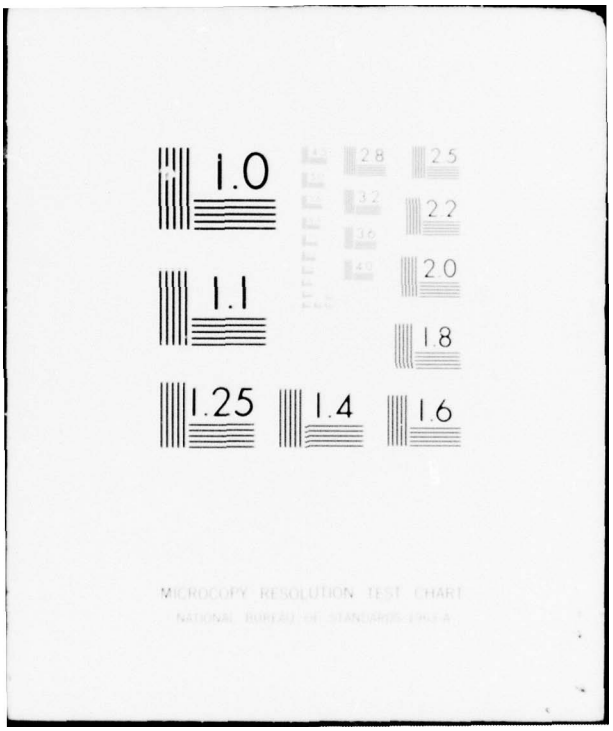
1.0
1.1
1.25
1.4
1.6
2.8
3.2
3.6
4.0
2.5
2.2
2.0
1.8
MICROCOPY RESOLUTION TEST CHART
NATIONAL BUREAU OF STANDARDS-1963-A

Report DAAG53-76-C-0162

(9)

TWO-DIMENSIONAL DIRECT ELECTRONIC FOURIER TRANSFORM (DEFT) DEVICES: ANALYSIS, FABRICATION, AND EVALUATION

Stephen T. Kowel
Philipp G. Kornreich
K. W. Loh
Amaresh Mahapatra
Moosa Mehter
Bruce Emmer
Paul Reck
William A. Penn

Dept. of Electrical and Computer Engineering
111 Link Hall
Syracuse University
Syracuse, New York 13210

30 June 1977

Interim Report for Period
10 June 76 - 9 June 77
approved for public release; distribution unlimited

Prepared for:

U.S. Army Night Vision Laboratory
Fort Belvoir, Virginia, 22060

SECURITY CLASSIFICATION OF THIS PAGE (When Data Entered)

REPORT DOCUMENTATION PAGE

READ INSTRUCTIONS BEFORE COMPLETING FORM

1. REPORT NUMBER: DAAG53-76-C-0162

2. GOVT ACCESSION NO.:

3. RECIPIENT'S CATALOG NUMBER:

4. TITLE (and Subtitle): Two-Dimensional Direct Electronic Fourier Transform (DEFT) Devices: Analysis, Fabrication, and Evaluation

5. TYPE OF REPORT & PERIOD COVERED: Interim Report 10 June 76 - 9 June 77

6. PERFORMING ORG. REPORT NUMBER: TR-77-5

7. AUTHOR(s): Stephen T. Kowel, Philipp G. Kornreich, K. W. Loh, Amaresh Mahapatra, Moosa Mehter, ~~Bruce Emmer, Paul Reck, and William A. Penn~~

8. CONTRACT OR GRANT NUMBER(s): DAAG53-76-C-0162

9. PERFORMING ORGANIZATION NAME AND ADDRESS:
Syracuse University
Electrical and Computer Engineering, 111 Link Hall
Syracuse, NY 13210

10. PROGRAM ELEMENT, PROJECT, TASK AREA & WORK UNIT NUMBERS:
15762709DH95
DA OD 3426

11. CONTROLLING OFFICE NAME AND ADDRESS:
US Army Night Vision Laboratory
DRSEL-NV-SD
Ft. Belvoir, VA 22060

12. REPORT DATE: 30 June 1977

13. NUMBER OF PAGES: 92

14. MONITORING AGENCY NAME & ADDRESS (if different from Controlling Office):

15. SECURITY CLASS. (of this report): unclassified

15a. DECLASSIFICATION/DOWNGRADING SCHEDULE:

16. DISTRIBUTION STATEMENT (of this Report)
Approved for public release; distribution unlinited.

17. DISTRIBUTION STATEMENT (of the abstract entered in Block 20, if different from Report)

18. SUPPLEMENTARY NOTES
Principal Investigators: Stephen T. Kowel, Philipp G. Kornreich

19. KEY WORDS (Continue on reverse side if necessary and identify by block number)

optics
acoustooptics
surface acoustic waves
Fourier theory
image analysis
spectral analysis
image transducers
image convolvers

20. ABSTRACT (Continue on reverse side if necessary and identify by block number)

We have fabricated an acoustooptical sensor capable of two-dimensional image or signal processing. It is a monolithic, optically addressed convolver, except that the two transducers propagate orthogonal, rather than colinear, surface waves. The interaction between image, acoustics, and electrons is obtained in a thin, polycrystalline film of CdS deposited on z-cut $LiNbO_3$. A double-layer technique produces reproducible, stable films with a 20% modulation of the photoconductivity proportional to the square of the SAW electric field. The signal current is detected by an interdigital contact pattern, made from an

DD FORM 1 JAN 73 1473 EDITION OF 1 NOV 65 IS OBSOLETE

Unclassified
SECURITY CLASSIFICATION OF THIS PAGE (When Data Entered)

406737 B

(20 cont.)

In/Al film sandwich deposited on the CdS.

With sinusoidal inputs, we obtain a difference frequency signal proportional to the spatial Fourier transform of the optical pattern focussed on the film. By varying the driving frequencies, we perform a vector scanning in Fourier space. Image rotation can be tracked electronically over a full 360°. The sensor can detect the spatial frequency, orientation, and amplitude of variations in the optical intensity. Phase measurements of the Fourier components, made by comparing the signal with an electronically synthesized difference frequency, show the expected linear variation with frequency, and the linear variation with displacement.

Other uses for the sensor would include line scanning, with pulses replacing sinusoids, and memory convolution with CdS CCDs made from the CdS film.

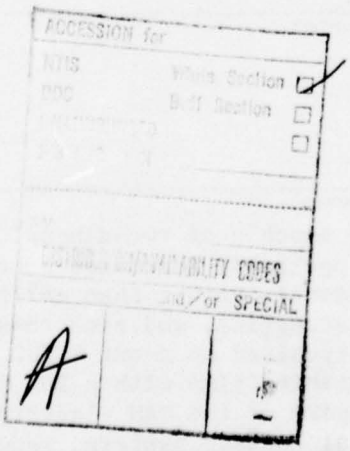

Report DAAG53-76-C-0162

TWO-DIMENSIONAL DIRECT ELECTRONIC FOURIER TRANSFORM (DEFT) DEVICES: ANALYSIS, FABRICATION, AND EVALUATION

Stephen T. Kowel
Philipp G. Kornreich
K. W. Loh
Amaresh Mahapatra
Moosa Mehter
Bruce Emmer
Paul Reck
William A. Penn

Dept. of Electrical and Computer Engineering
111 Link Hall
Syracuse University
Syracuse, New York 13210

30 June 1977

Interim Report for Period
10 June 76 - 9 June 77

Prepared for:

U.S. Army Night Vision Laboratory
Fort Belvoir, Virginia, 22060

TABLE OF CONTENTS

I. INTRODUCTION

This document serves as the interim report for the period 10 June 1976 to 9 June 1977 on the project entitled, "Direct Electronic Fourier Transforms of Images," funded by the U.S. Army Night Vision Laboratory. The original proposal was submitted to and approved by the Advanced Concept Team, U.S. Army.

An extensive literature already exists introducing DEFT technology to readers interested in both fundamental device development and applications.[1-9] Two recent papers on two-dimensional DEFT sensors are included as Appendices A and B for reference.

During this year's effort, DEFT technology made very significant strides. We substantially added to our knowledge of the fundamental nature of acoustooptical interactions in CdS. A successful method of fabricating high quality CdS films on $LiNbO_3$ was developed. This new method, involving layered films, yields stable films even on Z-cut $LiNbO_3$, whose temperature coefficient of expansion is much larger than other piezoelectric materials. Thus the films can be cured at high temperatures without cracking and peeling.

It was demonstrated that these films possess a large surface acoustic wave (SAW)—related conductivity modulation proportional to the square of the SAW—associated electric field in the $LiNbO_3$ substrate, as expected. Thus the modulation provided the pseudo-beam steering effect on which the two-dimensional Fourier transformation property rests.

With appropriate housing, coupling, and instrumentation, we were then able to obtain arbitrary two-dimensional Fourier components of images by fully electronic means. Measurements of spatial frequencies, their Fourier amplitudes and phase behavior, are reported here.

These are the first devices capable of two-dimensional signal processing using acoustic waves and employing no physical motion of the device or image. Of course, the devices on which this report is based need extensive improvements before they can be manufactured for practical use. Most of the sensor improvements needed to increase bandwidth, signal-to-noise ratio, and film uniformity, are already under way. Our analysis of these new sensors indicates that they could be used as correlators and convolvers. Indeed, it would seem that memory convolvers and correlators could be fabricated by forming an array of CdS charge-coupled devices (CCD) whose stored charges can interact with the travelling surface acoustic waves (SAW). Thus our current work on imaging could have an impact on signal processing, yielding signal/signal, image/-signal, and image/image correlation and convolution.

We also enhanced our understanding of the nature of the reconstruction problem. While several options exist, reconstruction of the picture from the transform signals appears to be the more complex task because of the memory function required. Devices, such as coherent light valves can use DEFT generated transforms to obtain the inverse transform optically but they are somewhat cumbersome and costly at present.

Experiments aimed at demonstrating pseudo-beam steering in a $LiNbO_3$ light valve sandwich structure are continuing. A number of problems have been indentified and corresponding improvements are being implemented.

The authors wish to extend their appreciation to Mr. David Helm of the Night Vision Laboratory, the project monitor, for his encouragement and active interest. We also wish to acknowledge the participation of Mr. Joseph Hannigan of the U.S. Army Engineer Topographic Laboratories, Fort Belvoir.

II. ELECTROPHOTOCONDUCTIVE SENSOR

In order to take full advantage of SAW Fourier imaging, it is essential to be able to electronically select arbitrary, two-dimensional, Fourier components of arbitrary, two-dimensional images. Previous work has been largely confined to obtaining one-dimensional transforms of one-dimensional[10,11] or two-dimensional images.[1,6,7] Various techniques have been proposed[1,12] for achieving full two-dimensional capability, culminating in the development of the pseudo beam steering technique discussed here.[4,8,9]

The direct electronic Fourier transform (DEFT) devices derive signals representative of Fourier components by acoustically modulating photoelectrons. In the electrophotoconductive device, two surface acoustic waves, travelling perpendicularly, cross the image, focused on a thin photoconductive film (CdS in the current model). It has been demonstrated that the absorption of light is strongly dependent on applied electric field, with the generated photocurrent having a component proportional to the square of the electric field.[13,14,15] We provide the electric fields by propagating the two crossed surface acoustic waves on a piezoelectric substrate ($LiNbO_3$) on which the CdS has been deposited. A full tensor treatment of the interaction reveals that the deposited contacts detect a current proportional to

$$i(t) \propto \iint dx\, dy\, E_z^2\,(x, y, t)\, I(x, y) \qquad (2.1)$$

where $I(x, y)$ is the image intensity, x and y are the coordinates on the film, and E_z is the electric field perpendicular to the plane.

Since

$$E_z = E_1 \cos(\omega_1 t - k_1 x) + E_2 \cos(\omega_2 t + k_2 y) \tag{2.2}$$

where E_1, ω_1, k_1, refer to the x-directed acoustic wave and E_2, ω_2, k_2, refer to the y-directed acoustic wave, E_z^2 contains a term of the form

$$\begin{aligned} E_{zd}^2 &\propto E_1 E_2 \cos[(\omega_1 - \omega_2)t - (k_1 x + k_2 y)] \\ &= E_1 E_2 \cos[(\omega_1 - \omega_2)t - \vec{k} \cdot \vec{r}]. \end{aligned} \tag{2.3}$$

By varying the driving frequencies, we can vary $\vec{k}$, yielding a signal term proportional to the two-dimensional Fourier transform,

$$i_s(t) \propto \exp[j(\omega_1 - \omega_2)t] \int d^{2\vec{r}} I(\vec{r}) \exp(-j\vec{k} \cdot \vec{r}) \tag{2.4}$$

while the other terms from (2.1) can be ignored because they are at different frequencies. That is, the signal behaves as if a new acoustic wave has been created with wavevector equal to the sum of the excited wavevectors. Thus we call this effect "pseudo beam steering."

From theoretical considerations alone, pseudo beam steering is likely to be far superior to other proposed techniques for accomplishing two-dimensional imaging. For example, the actual creation of a third surface wave from nonlinear mixing appears to be a much smaller and less controllable effect.[12]

The use of high frequency surface wave transducers requires that the image be placed on a high spatial frequency carrier. This is accomplished in one direction by the interdigital contact pattern used to detect the signal, and in the perpendicular direction by either etching the CdS into strips, or by projecting the image through a grid.

In this chapter, we first give a complete description of the operation of the sensor, referring to a phenomenological study of the conductivity

mechanisms. This is followed by a review of the many attempts to make adequate films of CdS on $LiNbO_3$, and a full description of the successful method finally developed. Included are the measured static and dynamic film properties and electron microscope studies of the surface.

After a brief discussion of the circuit and shielding problems, we present extensive experimental evidence from two operating sensors; one unidirectional and one fully two-dimensional. This includes measurement of spatial frequencies, amplitude and phase behavior. Convincing evidence of the pseudo-beam steering behavior is found in the data on image rotation. In these experiments, the physical rotation of an object, focused on the sensor, results in the expected disappearance of the Fourier component signal. The reaquisition of the signal by appropriate change of the transducer frequencies permitted the component to be tracked during a full 360° rotation.

The chapter concludes with plans for improvement in sensor design and electronic instrumentation.

II.1. Principles of Operation

The image sensor consists of a CdS film deposited on a z-cut $LiNbO_3$ substrate, as shown in Fig. 2.1.1. Thin film metal contacts, in the form of an interdigital pattern, are deposited onto the CdS film. This pattern permits the collection of the total photocurrent over the area of the CdS film. Indium is used as the contact material since it is our experience that indium makes ohmic contact to CdS.

Besides providing electrical contact, the contacts also form a coarse grating across the image. This, in effect, shifts the Fourier transform of the image along the k_y direction to higher spatial frequencies. It allows us to generate the Fourier transform of the image with SAW's having a limited bandwidth. A similar effect is obtained by etching the CdS film into strips along the x direction. We here use, for simplicity, gratings with equal dark and light spacings. Unfortunately, this type of grating only exposes 1/4 of the CdS film to the image. Larger film exposures are possible by making the dark areas of the masks narrower.

Since the photoconductivity of CdS has a term that depends on the square of the electric field, it is possible to obtain a mixing of the electric fields due to the two acoustic waves travelling perpendicularly to each other. This effect provides the effective steering of the wave vector corresponding to the spatial frequency of the transform.

Now let us use the following phenomenological approach to show how the two-dimensional Fourier transform of the image is obtained. In Appendix C we derive an expression for current density in the CdS film as a function of the light intensity $I(x, y)$, the D.C. electric field E_0 applied to the electrical contact, and the electric field E_μ due to the SAWs in the substrate.

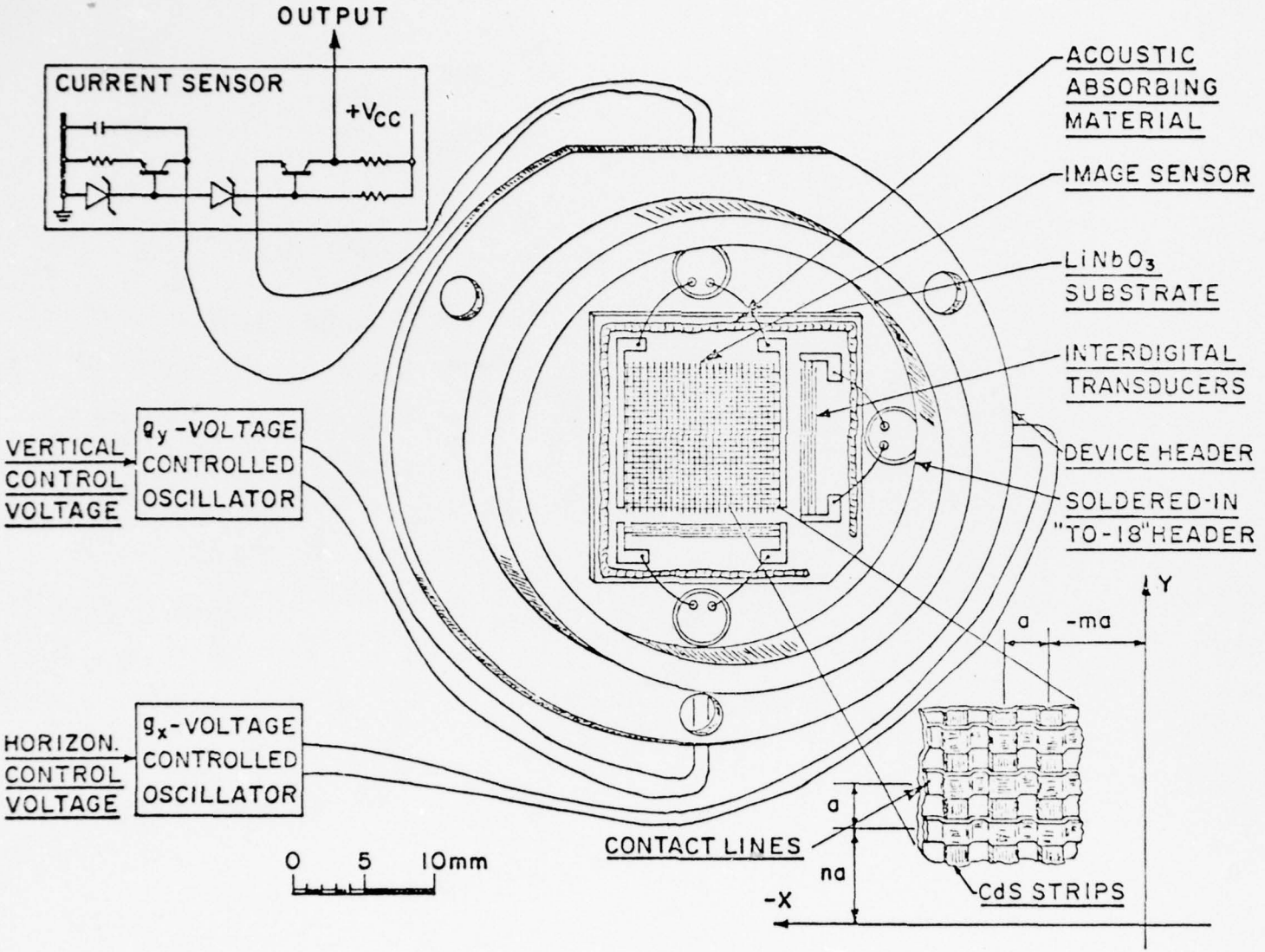

Fig. 2.1.1. Electrophotoconductive Sensor.

The details of the signal sensed at each small square of CdS are complicated by the fact that the light intensity, $I(x, y)$, may vary within each square. Also, the current detected is not proportional to the area of each square. For simplicity, let us first assume that the effect of the contact pattern and the etching of the CdS (or the projection of the image through a grid perpendicular to the contact lines) is to multiply the image intensity $I_i(x, y)$ by a sampling grid function, $S(x, y)$, and by an aperture function, $A(x, y)$, to form a new image, $I(x, y)$,

$$I(x, y) = I_i(x, y)S(x, y)A(x, y) \tag{2.1.1}$$

where $S(x, y)$ depends on the geometry of the sampling. The simplest model for S would be

$$\begin{aligned} S_1(x, y) &= ab\sum_{m=-\infty}^{\infty}\sum_{n=-\infty}^{\infty}\delta(x - ma)\delta(y - nb) \\ &= ab\sum_{m=-\infty}^{\infty}\sum_{n=-\infty}^{\infty}\delta(x - ma, y - nb) \\ &= \mathrm{comb}(x/a)\ \mathrm{comb}(y/b). \end{aligned} \tag{2.1.2}$$

Fig. (2.1.1) shows the special case for which $b = a$, providing uniform sampling in both directions. As we shall see, there are possible advantages in having $b \neq a$, but all devices built so far do have $b = a$.

A more realistic sampling function for the sensor is obtained by breaking the image into squares,

$$S_2(x, y) = \mathrm{rect}_{a/2}(x)\ \mathrm{rect}_{b/2}(y) * S_1(x, y) \tag{2.1.3}$$

where * indicates convolution and

$$\text{rect}_{a/2}(x) = \begin{cases} 1 & |x| \leq a/2 \\ 0 & |x| > a/2 \ . \end{cases} \tag{2.1.4}$$

Next we note that the image space is truncated by a device aperture function, $A(x, y)$, given by

$$A(x, y) = \text{rect}_{Ma}(x)\ \text{rect}_{Nb}(y) \tag{2.1.5}$$

where (Ma)(Nb) is the total area of the CdS film spanned by the contacts. Thus the final image is

$$I(x, y) = I_i(x, y)[\text{rect}_{Ma}(x)\text{rect}_{Nb}(y)]. \\ [\text{comb}(x/a)\ \text{comb}(y/b)] * [\text{rect}_{a/2}(x)\text{rect}_{b/2}(y)]. \tag{2.1.6}$$

Now we are in a position to calculate the detected signal current for the image of (2.1.6). The surface current density at the difference frequency is given by (C.11). The detected current is

$$i_{sig}(t) = \sum_{\ell=-\infty}^{\infty} \int_{-\infty}^{\infty} dx\ K_{sig}(x, \ell b, t) \tag{2.1.7}$$

since the current is sampled at specific points along the y-direction by the contacts, rather than being measured at all points between the contacts. We use infinite limits here since we include the sensor geometry in the expression for the $I(x, y)$. Now since the principal value of the two-dimensional sampling is to put the original image I_i on a spatial carrier whose periods are a and b in the x and y directions respectively, it is reasonable to assume that I_i only varies appreciably over many squares. In this case the sum in ℓ can be replaced by an integration,

$$i_{sig}(t) = \frac{1}{b} \int_{-\infty}^{\infty} dy \int_{-\infty}^{\infty} dx \, K_{sig}(x, y, t) \tag{2.1.8}$$

which we can write as a complex phasor current

$$i \alpha \frac{1}{b} \int_{-\infty}^{\infty} dy \int_{-\infty}^{\infty} dx \, I(x, y) \exp -j(k_x x + k_y y) \tag{2.1.9}$$

$$\alpha \frac{1}{b} F\{I(x, y)\}. \tag{2.1.10}$$

Let us now examine $F\{I(x, y)\}$, from (2.1.1)

$$F\{I(x, y)\} = \mathcal{I}_i(f_x, f_y) * S_2(f_x, f_y) * A(f_x, f_y) \tag{2.1.11}$$

where $f_x = k_x/2\pi$, $f_y = k_y/2\pi$, spatial frequencies normally used in Fourier optics [20], and the functions $\mathcal{I}$, S, and A are the respective Fourier transforms of the functions I, S, and A. We see at once that

$$\mathcal{I}_i(f_x, f_y) * S_2(f_x, f_y) = \mathcal{I}_i * \left[S_1 \cdot \frac{\sin \pi f_x a/2}{\pi f_x} \cdot \frac{\sin \pi f_y b/2}{\pi f_y}\right] \tag{2.1.12}$$

yielding,

$$\left[\frac{\sin \pi f_x a/2}{\pi f_x} \cdot \frac{\sin \pi f_y b/2}{\pi f_y}\right] \cdot \left[\mathcal{I}_i(f_x, f_y) * (ab) \operatorname{comb}(af_x) \operatorname{comb}(bf_y)\right] \tag{2.1.13}$$

$$= \left(\frac{\sin \pi f_x a/2}{\pi f_x}\right)\left(\frac{\sin \pi f_y b/2}{\pi f_y}\right) \left[\mathcal{I}_s(f_x, f_y)\right] \tag{2.1.14}$$

where

$$\mathcal{I}_s(f_x, f_y) = \sum_{m=-\infty}^{\infty} \sum_{n=-\infty}^{\infty} \mathcal{I}_i\left(f_x - \frac{m}{a}, f_y - \frac{n}{b}\right). \tag{2.1.15}$$

Thus the effect of sampling is to reproduce the image transform over and over again. With b = a, these reproductions are centered at (0, 0), (1/a, 1/a), (-1/a, -1/a), etc.

We chose to operate with transducers whose center frequencies correspond to spatial frequency (1/a, 1/a) and which have a bandwidth of approximately 20%. It is important that the image transform I_i have a bandwidth limited to approximately the same 20% otherwise the replications will overlap and cause distortion. This statement is equivalent to our previous assumption of slowly spatially varying $I_i(x, y)$.

Note also the effect of the rectangular nature of the actual sampling grid. It serves to envelope the transform with a sinc function along each axis whose local maximum coincides with the centers of the replicated spaces as shown in (2.1.14).

It is convenient to define the space centered at (1/a, 1/a) as the reduced Fourier space by introducing g_x, g_y, where

$$f_x = \frac{1}{a} + g_x \tag{2.1.16}$$

and

$$f_y = \frac{1}{a} + g_y \ . \tag{2.1.17}$$

The effect of sampling can now be written as

$$I_s(f_x, f_y) = I_i(g_x, g_y). \tag{2.1.18}$$

Now we can include the last factor in $I(f_x, f_y)$ from (2.1.1), the effect of the finite device aperture. From (2.1.11),

$$I(f_x, f_y) = I_i(g_x, g_y) * \left[\frac{\sin \pi Maf_x}{\pi f_x} \cdot \frac{\sin \pi Maf_y}{\pi f_y}\right] \tag{2.1.19}$$

where we assume a square sensor contact region, Ma on a side. Thus the effect of the finite device size is to smooth the reduced Fourier space

with a sinc function which is reduced to 1% of its center value (for M = 100) at the edge of the space. The main lobe has a bandwidth of 1% of the center frequency which implies that data will be smoothed out over one percent of the center frequency. Indeed, this is observed in the devices. It is interesting, in this regard, to note the Shannon-Whittaker Sampling Theorem[20], which states that, for a space limited function, evenly spaced samples in frequency space, separated by (1/Ma), will suffice to completely characterize the function. This is the smoothing width! Therefore, it is theoretically possible to reconstruct the function $I_i(x, y)$. In practice, however, the fact that the current detected at each square of CdS is an averaged version of the optical intensity over the square, the fact that the sampling in real space produces possibly overlapping reduced spaces, and finite bandwidth all prevent precise reconstruction.

Finally, then, we have that the signal current phasor at the difference temperal frequency $(\omega_1 - \omega_2)$ is

$$i = \frac{1}{b} (\sigma_{13}^{LE} + \sigma_{66}^{LE}) E_{1z} E_{2z} E_0 \quad \bar{I}_i(g_x, g_y) \cdot \tag{2.1.20}$$

$$\cdot \frac{\sin \pi f_x/2}{\pi f_x/2} \cdot \frac{\sin \pi f_y/2}{\pi f_y/2} \tag{2.1.20}$$

where we introduce standard elasticity notation from Appendix C, and define $\bar{I}$ as the smoothed version of the transform of the image intensity (2.1.19).

From (C.10) we calculate the bias, or d.c., value of the current to be

$$i_{d.c.} = \frac{1}{b} \int_{-\infty}^{\infty} dy \int_{-\infty}^{\infty} dx \, K_{y0}(x, y, t) \tag{2.1.21}$$

$$= \frac{1}{b} \sigma_d E_0 \int_{-\infty}^{\infty} dy \int_{-\infty}^{\infty} I(x, y) dx \tag{2.1.22}$$

where

$$\sigma_d = \sigma_L + \sigma_{11}^{LE} E_0^2 + \frac{1}{2} (\sigma_{44}^{LE} + \sigma_{12}^{LE}) E_{1x}^2 + \frac{3}{2} \sigma_{11}^{LE} E_{1y}^2$$

$$+ \frac{1}{2} (\sigma_{13}^{LE} + \sigma_{66}^{LE}) (E_{1z}^2 + E_{2z}^2) \tag{2.1.23}$$

Substituting (2.1.22) into (2.1.20) eliminates E_0 to yield

$$i = i_{d.c.} \frac{(\sigma_{13}^{LE} + \sigma_{66}^{LE})}{\sigma_d} E_{1z} E_{2z} < \overline{I}_i(g_x, g_y) > \cdot \cdot \frac{\sin \pi f_x/2}{\pi f_x/2} \cdot \frac{\sin \pi f_y/2}{\pi f_y/2} \quad (2.1.24)$$

where

$$< \overline{I}_i > \equiv \overline{I}_i / \int_{-\infty}^{\infty} dx \int_{-\infty}^{\infty} dy \; I(x, y). \quad (2.1.25)$$

Thus we have completed our model showing how the geometry of the sensor when properly coupled to the acoustics yields a two-dimensional Fourier transform of the image. It is interesting to note that a choice of $S(x, y)$ which uses the same sampling rate in both directions results in the situation that, for $\omega_1 = \omega_2$, no output is obtained unless very special circuits are employed to measure this d.c. signal. Thus the transform components along the line $g_x = g_y$ will not be obtained. This problem can be avoided by using a/b equal to an irrational number sufficiently large to make this line pass outside of the reduced space. Fig. (2.1.1) and Fig. (2.1.2) show the f_x, f_y and g_x, g_y spaces schematically. Next we discuss the experimental confirmation of this theory.

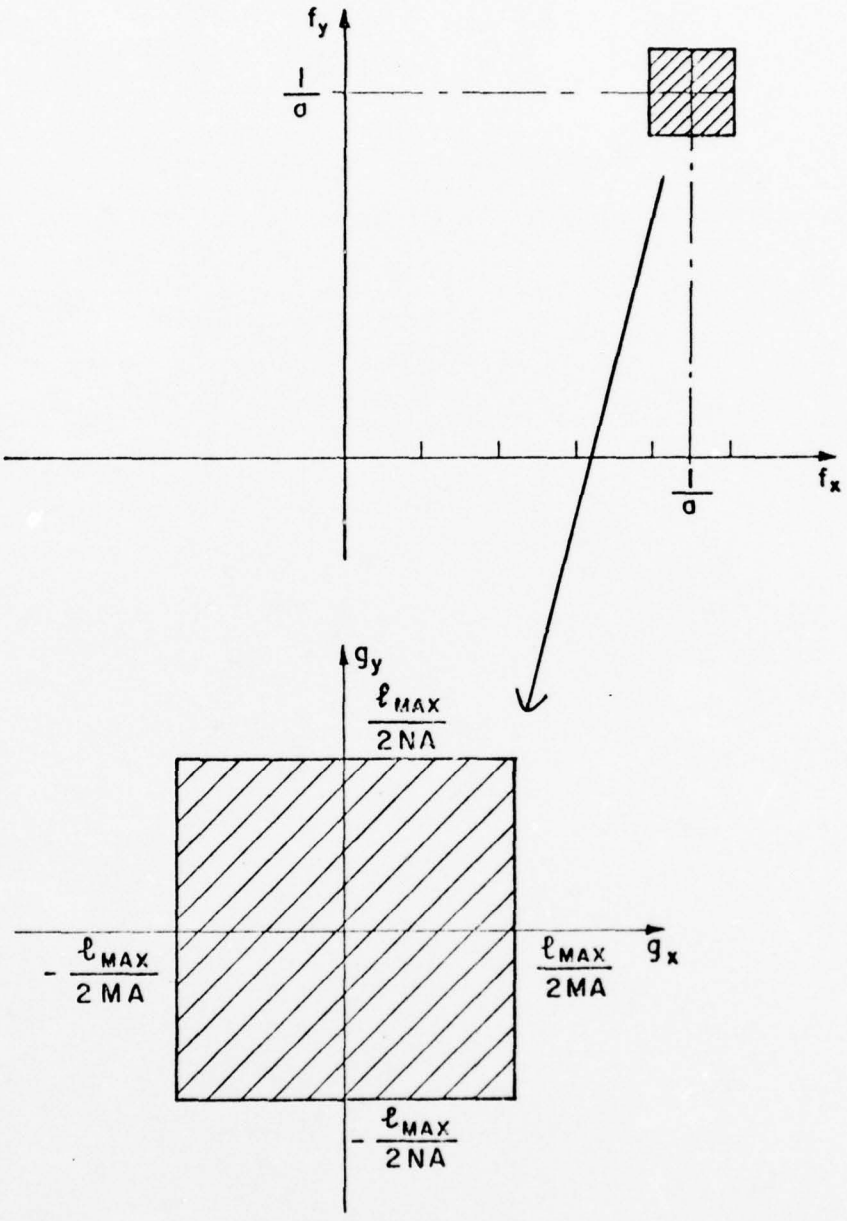

Fig. 2.1.2 Schematic representatation of the original Fourier space (f_x, f_y) and the reduced Fourier space (g_x, g_y). The value of ℓ^2_{max} is the number of Fourier components available in the reduced space and is determined by transducer design.

II. 2. Layered CdS Film Deposition and Curing

The most difficult task encountered was the production of good photoconductive thin films of CdS. Since we had been making such films on glass for several years, we had hoped that the technique for making the films could be used relatively intact. (Glass cannot be used as a substrate since there is no travelling electric field accompanying the SAW.) Unfortunately, this did not prove to be the case.

On the glass substrates CdS was evaporated out of a fused quartz bottle onto suitably positioned substrates in a vacuum of 10^{-5} Torr. These evaporated films had very high conductivity but a poor light-to-dark conductivity ratio. To increase their sensitivity they were cured at 650° C under a N_2 flow which had traces of O_2, HCl, and Cu, to optimize the photoconducting properties of the films. We finally succeeded in obtaining L/D ratios of about 10^3 at 275 m.cd. At the same time, the conductivity of the films was quite high, about 0.1 nanomho/□-m.cd. This is essential to obtain reasonable signals with sensor contact lines having about 20,000 squares in parallel.

We hoped that by suitably adjusting the doping levels of O_2, HCl and Cu, one could get good photoconducting films of CdS on $LiNbO_3$. However, after numerous attempts, we came to the conclusion that this is not possible due to the degrading effects of material diffusing out of the $LiNbO_3$ during curing.

Next, we decided to overcome the problem of the substrate entirely, by laying down a thin layer of SiO_2 between the substrate and the CdS film. This layer would insulate the CdS from the $LiNbO_3$. At the same time, SiO_2 being stable thermally, would not itself diffuse into the CdS. This idea proved successful in that we improved the L/D ratios by a factor of 100 in our first attempts.

Unfortunately, the SiO_2 layer had its own problems. It worked fairly well with y-cut $LiNbO_3$, which has a low coefficient of thermal expansion like the SiO_2. But on z-cut $LiNbO_3$, which has a coefficient of thermal expansion 10 times that of y-cut, the films peeled off during curing.

At this point, a number of attempts to prevent the CdS from peeling off the SiO_2 were made, such as graduating the SiO_2 - CdS boundary during evaporation, and roughening the surface of the $LiNbO_3$. All of these were unsuccessful. We also tried to out-diffuse the $LiNbO_3$ before evaporation. This would obviate the need for the SiO_2 film. This was also unsuccessful. The films were still degraded during curing.

We also tried Al_2O_3 as an intermediary diffussion barrier. Unfortunately the CdS film peeled off the Al_2O_3 just as it did from SiO_2. Attempts to prevent peeling by making very thick thin films of SiO_2 to allow for different expansion rates on the opposite sides were also unsuccessful.

Eventually we struck upon the ideal solution. We knew that CdS itself would stick to $LiNbO_3$. Therefore why not insulate the photoconducting CdS film from the $LiNbO_3$ by a second CdS film. If this film were thick enough it would not permit out-diffused elements from $LiNbO_3$ to reach the second film of CdS. Moreover, there would be no sticking problem at either surface. Our very first experiment with this technique yielded very good L/D ratios. It soon became clear that one could easily adjust the doping levels of HCl, O_2 and Cu for the second CdS film to have L/D ratios of 10^4 at 500 m.cd.

Since then we had made a number of CdS films on $LiNbO_3$ by this "double-deposition", or layered, technique. Reproducibility and film uniformity remain less than ideal essentially because our doping techniques are still rather crude.

Appendix D reveals the "recipe" for evaporating and curing the films.

It should be noted that these films represent the first reliable photoconductive films on $LiNbO_3$ or, as far as we know, on any other piezoelectric substrate. Luukala[11] has made CdSe films on y-cut $LiNbO_3$ but has reported great difficulty in reproducing these films because of cracking and peeling[19].

II.3 Measurements of CdS Film Properties

Once the CdS films have been laid down and cured, it is of considerable interest to study a number of parameters that can be correlated with known and predicted properties. These include surface uniformity, absorption of light as a function of optical wavelength, conductivity change as a function of light level, change of conductivity with strain, and change of conductivity with temperature. In this section we describe a number of such measurements and correlate the results, whenever possible, with our expectations.

II.3.1. Film Thickness

Only recently we established an optics facility including a pneumatically-isolated table (4 ft. x 8 ft.), associated hardware and lasers, and a high sensitivity spectroradiometer.

Using the table, we were able to set up a simple Michelson interferometer in order to measure the thickness of the CdS films. We had for years assumed that the CdS was approximately 10μ. To determine the true thickness, we deposited a film on glass through a mask that produced an abrupt edge. We then deposited aluminum over the film so that this metal film uniformly covered the region on both sides of the abrupt edge. By using this aluminum film as one mirror in the Michelson interferometer, an interference pattern was formed on a screen. With care, the difference in the length of the paths from the "test" mirror and a standard first surface mirror could be adjusted to be a few wavelengths of light. We thus observed a pattern containing between three and six fringes. The patern was split in the middle because of the abrupt junction. A shift of 0.5 fringes was observed across the pattern due to the CdS film.

Using the result[22]

$$\text{distance moved} = (\#\text{ of fringes displaced})\left(\frac{\lambda}{2}\right)$$
$$= (\text{CdS film thickness}) \qquad (2.3.1.)$$

for a wavelength of 6328Å, we estimate the film thickness to be 1582Å.

An alternate method based on the geometry of the evaporation process was also used. Assuming uniform evaporation over a hemisphere and knowing the total amount of CdS evaporated yields a thickness of approximately 2300Å. Using the Inficon Deposition Rate Monitor indicates a film thickness of 4500Å but its sensor is only 2/3 as far from the evaporation boat as is the substrate which implies a thickness of 4500Å (4/9) = 2000Å.

In any case, these films are much thinner than expected. Thus it is possible that still larger conductivities can be obtained by longer evaporations. Of course, on $LiNbO_3$ the total thickness of the two layers is twice the thickness measured in these experiments.

II.3.2. Surface Properties

The films were examined under an electron microscope at various stages of fabrication. The surface of the bottom film is smooth with no obvious structure. On a 1μ scale it looks something like rough concrete. Once cured, a definite crystallization becomes evident. The film looks like a tile floor with irregularly shaped but smoothly fitting tiles. On top of the film is what appears to be excess CdS dust. The crystallites have between four and six sides and are between one-half to one micron in diameter.

With the second layer deposited, the surface looks very hilly and irregular. But after curing, we are again left with a smooth film with clear crystallite boundaries, although not as smooth as the bottom film. Fig. (2.3.1.) shows the surface of this final film. Notice that again there is dust sprinkled on top of the film. We are giving some thought to see whether this curing artifact can be prevented or removed. It is quite significant that there are no holes or tears in the film even though it is quite thin.

II.3.3. Film Conductivity

We have measured the i-V characteristics of CdS films on $LiNbO_3$. The voltage was varied over 4 decades and the i-V curve was found to be linear. The contact separation was about 75μ. Assuming the crystallites to be 1μ wide, there were 75 crystallites between any pair of contacts. Let us assume that the barrier model of conductivity holds for our films, so that we can assume the current to be of the form

$$i = I_0(\exp(-\phi/kT)[\exp(qV_d/kT) - 1] \qquad (2.3.2.1)$$

where ϕ is barrier voltage between crystallites, and V_d is the drift voltage across each barrier[18]. Now if $qV_d \leq kT$, the above expression can be suitably expanded to give a linear i-V characteristic. However, at the highest applied voltage we used (20 V), V_d is about $20/75 \cong .267$ V. Thus qV_d is about 10 times kT and one would expect highly non-linear i-V curves. Since this does not happen, we think that either the barrier model does not apply to our films or (2.3.3.1), quoted in may papers, is an over simplification. Appendix E describes an alternative theory which does agree with our data.

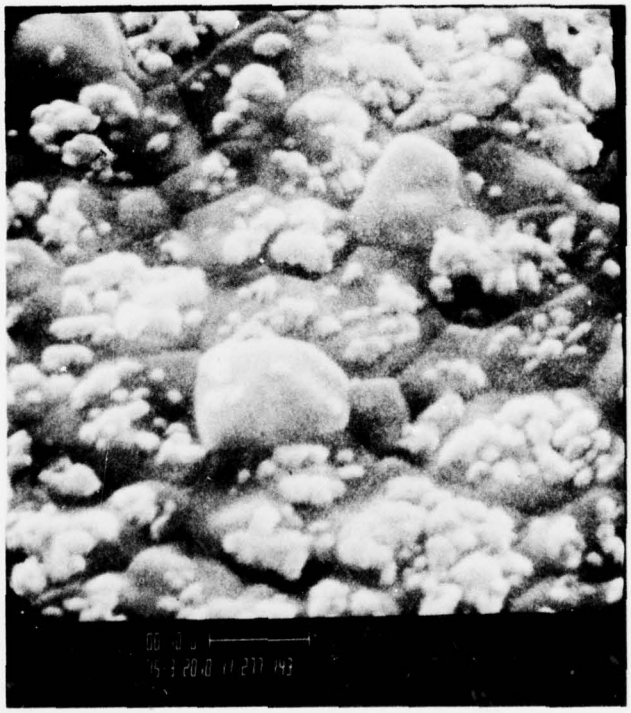

Fig. 2.3.1. Scanning electron microscope study of the finished film. Note the 1 μ scale indicated just under the picture.

We obtained a linear curve for current versus voltage from V = 0.002 V to V = 20 volts, i.e., over 4 decades. The drift-electric field changes from E = 0.2 V/cm to E = 2 x 10^3 V/cm.

We next measured the variation of photocurrent with light wavelength. The normalized curve, given in Fig. 2.3.2, shows the band edge to be at 505 nm which corresponds to a band gap of 2.46 V. The photocurrent drops sharply at higher wavelengths. However, there is a secondary maxima at 560nm, which corresponds to a level 0.25 V from the valence band. A similar level was detected in our CdS films on glass. We believe this to be a sensitizing center with low capture cross-section for electrons. These measurements were made using the new E.G. and G. High Sensitivity Spectroradiometer.

The next measurement was the variation of photocurrent with white light intensity, showing clearly the power-law behavior of the conductivity. There is a supralinear variation with an exponent 1.4. However, our films on glass had an exponent lying between 0.8 and 1, probably due to sensitizing centre lying closer to the valence band (0.15 ev). We also measured the rise and decay times of the photocurrent for different white light intensities from 40 to 10^3 m.cd. The rise, as expected is an order of magnitude larger than the decay time. The decay time changes from 28 msec at low intensities to 3 msec at 10^3 m.cd. From the decay time one can calculate the trap density at the position of the Fermi level. $N_t kT$ seems to be about 5 x 10^{15} cm^{-3} at a distance of about 0.45 e.v. from the conduction band. To investigate trap densities closer to the conduction band one would have to perform cryogenic measurements.

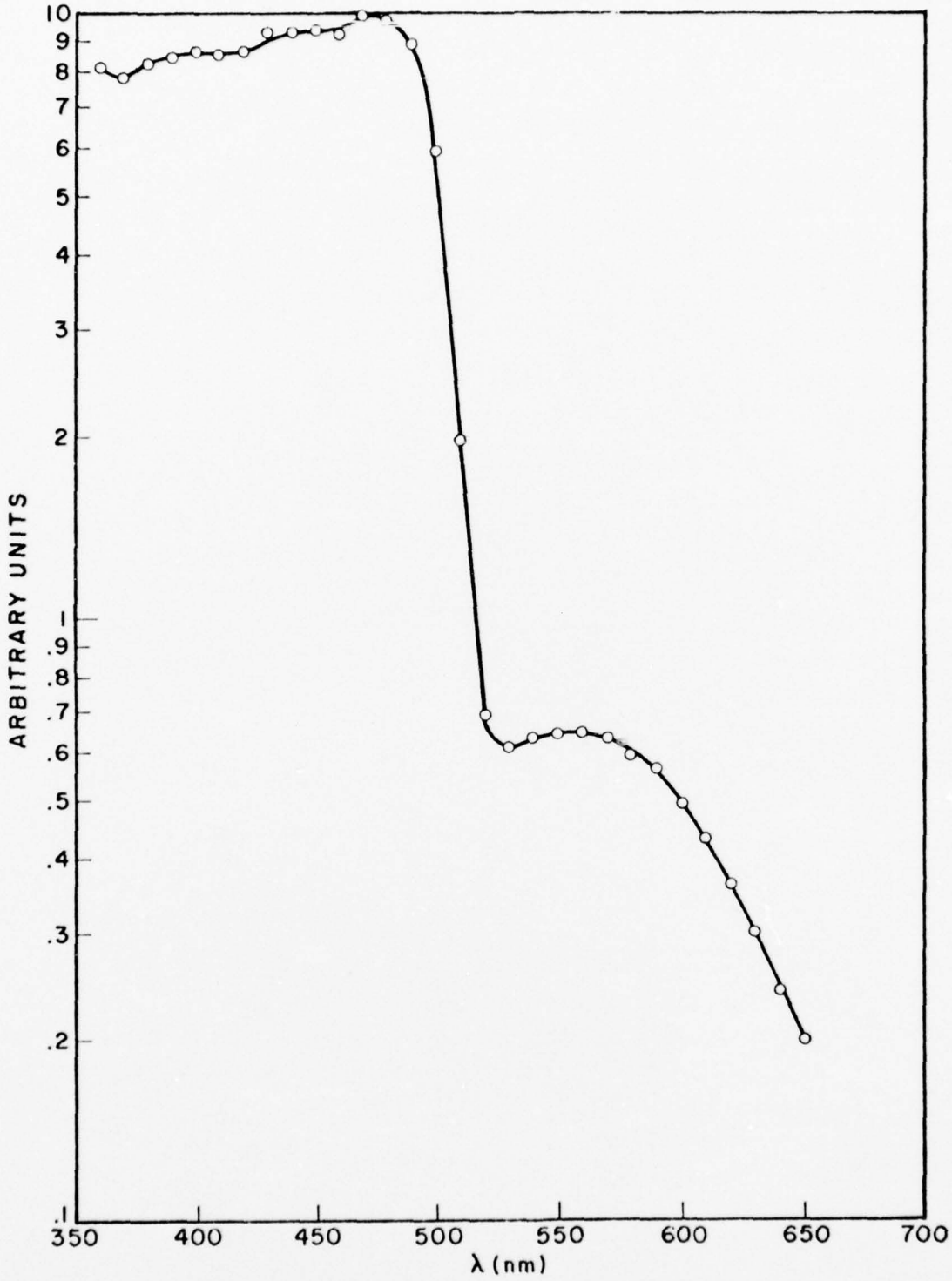

Fig. 2.3.2. Variation of Photocurrent with Light Wavelength

II.4. Experimental Confirmation of Pseudo Beam Steering and Fourier Imaging

The successful fabrication of the CdS films is merely one crucial step in building a sensor. The next step is the metallization. By this we mean the process of producing contacts which serve as bias and signal detection ports as well as transducers. In addition, the substrate may require metallization for shielding purposes. These steps complete the sensor. Next comes a challenging problem in circuit design to enable the extraction and amplification of the signal.

Work on all three aspects (CdS, metallization, circuits) has proceeded in parallel. During the Summer of 1976, we designed a self-contained system using voltage-controlled oscillators for scanning Fourier space. We tested several sensors with this system but the results were ambiguous since the sensors were very poor. At that time our films all suffered from either peeling or poor light sensitivity. We did, however, make some measurements and report them. The description of these experiments and their results may be found in Appendix B. Among the conclusions was the fact that the circuits designed for driving the transducers so as to provide circular sweeps through Fourier space needed to be significantly improved for quantitative use. For this reason, we decided to concentrate on improving the sensor and to use test equipment to evaluate performance rather than concern ourselves with circuit improvements.

Once good films were available, our first problem was metallization. We observed years ago that indium makes good ohmic contact to CdS while aluminum, the material normally used in SAW technology, does not. Also,

we cannot use the "etching" technique to fashion the metal fingers from the vacuum—deposited metal film. Any etchant that will remove metal will remove CdS. Thus we had to learn a more sophisticated technique known as the "lift-off" method.[23]

In order to produce the metallization by lift-off, one prepares the CdS film as discussed in Section II.2. After cleaning, photoresist is spun on using a centrifugal platform. This photoresist is then exposed in a mask aligner to an optical pattern provided in the shape of the wanted metallization. The resist is then developed and washed. This leaves behind a pattern of resist. Then the indium metal is vacuum deposited and washed with acetone. If the deposition is properly done, some indium will sit on top of the resist lines, and some will sit in the valleys. As long as the photoresist is thicker than the indium and the indium "beam" is highly "collimated" during evaporation, the indium film will be segmented. The acetone can then burrow into the resist lines from the edges and "lift" away the resist and the metal resting on top. This leaves the low-lying metal lines intact.

Unfortunately, indium films thin enough for lift-off turned out to have a very poor conductivity. This is a serious problem because of the length of our finger patterns. We solved this problem by a thin film of aluminum on top of the indium film. Such sandwich films permit the indium to make ohmic contact to the CdS, while the aluminum films permit the long surface conduction route. The details of these steps are still undergoing improvement at this time.

One problem still remains because of the need for the image to be sampled in both directions. The metal sandwich samples along one direction. Either an external grid running perpendicularly to the metal

lines must be suspended just above the sensor, or else the CdS itself must be etched into lines before using the lift-off technique.

Both methods have advantages. Etching the CdS film produces some degradation and introduces a small non-uniform acoustic mass loading. It also encodes the dark current on the same carrier as the optical signal. On the other hand, the projected grid is somewhat inconvenient.

The most significant factor until the present, however, is the fact that with the etched films, the lift-off is much more difficult due to the non-uniform surface for the photoresist to spread over. Fig. (2.4.1) shows the typical result when etched CdS is used. The CdS (black vertical lines) is not completely covered by the metal lines (white horizontal lines). At the upper left and lower right, small sections of the transducer contacts can be seen. At the lower left, the contact pattern and the CdS fingers are evident. The metal contact fingers are broken at the steep edges of the CdS film. We are working to prevent this by adjusting the various thicknesses. Thus all successful devices are of the projected grid variety.

The photograph shows clearly that the sampling of the image corresponds to one sample per acoustic wavelength in each direction. The distance between active CdS "squares" equals the period of the transducer pattern. These sensors have 100 x 100 CdS squares covering an area of 12 mm x 12 mm. The whole sensor fits on one half of a two-inch diameter $LiNbO_3$ wafer. The transducers contain 15 finger-pairs and are apodized with a sinc function overlap.

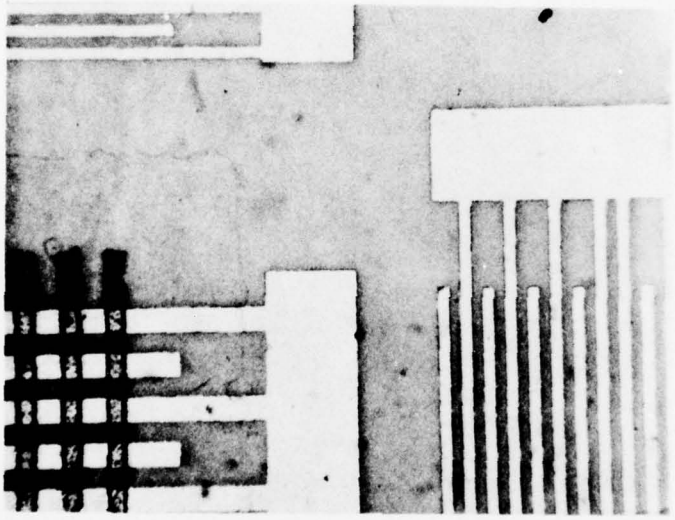

Fig. 2.4.1. Small Segment of Etched CdS Film Device.

II. 4.1. Unidirectional Sensor

The first truly successful device was a unidirectional sensor based on the principles and fabrication techniques described. This device was built since it was deemed easier to evaluate than a full two-dimensional system. The crystal was subjected to x-ray analysis. We were able to identify the x and y axes of the wafer by comparing our pictures to published data[24]. The wafer was cut in half along a line 13.5° from the true x-axis. This cut became the "x-axis" referred to in all of the previous equations. This axis was choosen since it yields the most identical acoustic behavior to its orthogonal axis, which we have referred to as our "y-axis."

In this first sensor four transducers were fabricated, two on each side of the CdS film/contact region. These transducers were made from the same mask as those mentioned above. They had center frequencies of 28.2 MHz and a useable bandwidth of 4.0 MHz. Acoustic insertion loss measurements were made by exciting one transducer and detecting the delayed signal at the farthest transducer. Since we observed a 40 dB loss, we decided to tune out the transducer capacitance using small ferrite-filled adjustable inductors. Using an r.f. impedance meter, we determined the required inductance to be approximately 1μh. With matching, the insertion loss was reduced to 18 dB, a very respectable figure.

In a unidirectional device, one has to measure either the sum or difference frequency. The capacitance of the contact pattern made measurement of the sum ($\simeq$ 60 MHz) an unappealing choice. Thus the device was operated without sampling along the x-direction, and excited by two transducers on the same side of the CdS/contact region. In this case, in place of (2.1.24), we obtain

$$i(t) \alpha \exp j(\omega_1 - \omega_2)t < \overline{T}_i(f_{x1} - f_{x2}) > \qquad (2.4.1)$$

where f_{x1}, f_{x2}, are the spatial frequencies of the acoustic waves at radian temporal frequencies ω_1, ω_2, respectively. Thus we obtain base-band spatial components without sampling.

Our first attempts to measure the signals were not successful. An enormous feedthrough signal presented itself. We were quite disappointed as we had naively expected that feedthrough at 30 MHz would be nicely removed by a low-pass filter in the detector, leaving us with a low difference frequency. Unfortunately, the 30 MHz signals were so large that mixing was occurring in the detection electronics. This was largely solved by depositing an aluminium film on the bottom surface of the substrate, grounding it effectively, and by grounding one side of each transducer to it. This reduced the r.f. fields straying into the contact area.

Even with attention to shielding, we still observed image independent difference frequency signals. There appear to be two methods that could reduce this further. One is to operate the device in a gated mode, using the surface wave delay property to detect the signal during the time when the transducers are not being driven. This requires a separation between closest transducer and the CdS/contact region of at least two contact pattern lengths. At the time, we were unable to fabricate a device with that much "open space".

The other alternative was to build a very selective low-pass filter to be inserted directly at the contact terminal port, rather than at the detector output. Such a filter, with 60 dB separation between 30 MHz and the desired signals (between zero and 4 MHz), did effectively put an end to the feedthrough problem.

With these improvements, we were able to detect the long hoped for difference frequency signal which was image dependent, and disappeared in the dark. The device was operated with the bias current electronically maintained at a constant level of 0.25 mA. The sensor, with a resistance of 1KΩ, acted like a current source since it was terminated in 15Ω.

In a typical experiment, one transducer was tuned to 28.2 MHz, while the other was swept between 26.13 MHz and 31.33 MHz. Grid patterns were illuminated by an 8 milliwatt HeNe laser and focused on the CdS film. Periodic grids were chosen whose spatial frequency corresponded to the available values of $f_{x1} - f_{x2}$. A typical output is shown in Fig. 2.4.2. The upper trace is for a grid with period 2.08 mm and the lower trace is for a grid with period 3.47 mm. The center portion of both traces represents the average value of the light intensity, zero spatial frequency. It is a sinc function whose width (0.3 MHz) is the same as the high frequency peaks due to the aperture smoothing effect. The center null in the zero component is an artifact of the detection electronics having a low frequency cut-off.

Since we have a wave vector $k_{1x} - k_{2x}$ and a radian frequency $\omega_1 - \omega_2$, the effective "velocity" of this pseudo wave is

$$v_p = \frac{\omega_1 - \omega_2}{k_1 - k_2} = \frac{v_R(k_1 - k_2)}{k_1 - k_2} = v_R \qquad (2.4.2)$$

where v_R is the Rayleigh wave velocity of each acoustic wave. For z-cut $LiNbO_3$ with "x-directed" waves, $v_R \simeq 3820$ m/s. This tells us that an object with a spatial period of 2.08 mm should be imaged when

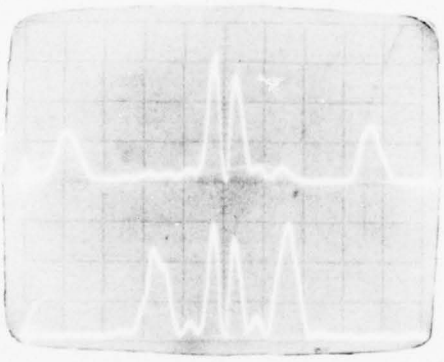

Fig. 2.4.2. Typical Results Using the Unidirectional Electrophotoconductive Sensor. The traces represent amplitude as a function of spatial frequency.

$$\Delta f = v_R(f_{x1} - f_{x2}) = v_R \Delta f_x = \frac{3820}{.00208} = 1.84 \text{ MHz} \qquad (2.4.3)$$

where Δf is the measured difference temporal frequency. Indeed, the peaks in the upper trace were centered at $\pm$ 1.84 MHz.

If an imaged grid was expanded and contracted by the use of a telescope, the twin peaks moved in and out just as expected.

Thus we were convinced that the electrophotoconductive effect was significant and yielding the expected Fourier behavior. We studied the magnitude of the measured modulation of the photoconductivity and found that our acoustically induced signals correspond to $\sigma^{LE}E^2/\sigma^L \approx 0.2$, i.e., a 20% modulation of the photoconductivity. This is a remarkably large nonlinearity and represents a significant physical measurement quite apart from its information processing aspects.

It is also worth noting that these measurements correspond to acoustic power densities of $\approx$ 4 milliwatts per mm of aperture and is achieved with driving voltages of a few volts. The modulation was linear as a function of $\sqrt{P_1 P_2}$ where P_1, P_2 are the acoustic powers generated at the two transducers.

II. 4.2. The Two-Dimensional Sensor

Based on the success of the unidirectional sensor, we fabricated a two-dimensional sensor such as shown in Fig. 2.1.1. As pointed out in Section II.4 the actual sensor is at present fabricated using an unetched CdS film. A contact pattern is metallized on a thin glass plate which is supported just above the substrate by tape. These metal lines are perpendicular to the CdS contacts lines and thus provide the required image sampling.

This sensor requires all of the improvements described in the previous section. It is mounted in an aluminum box with an opening for the light. No lens is used on the box at present since we can project good quality images using a beam of coherent light (6328Å).

Fig. 2.4.3 shows the schematic representation of the test set-up. The orthogonal transducers generate the acoustic waves because of the piezoelectric nature of the $LiNbO_3$. As in the unidirectional sensor, the metal finger patterns produce electric fields which then couple to the substrate exciting Rayleigh waves.

The experiments performed were meant to give convincing proof that the strong acoustically induced modulation of the photoconductivity did produce the pseudo beam steering effect required for two-dimensional transform imaging. Basically this required us to do experiments similar to those performed on the unidirectional device, and then show that as the image is physically rotated, the device can electronically track the image spatial components angle for angle.

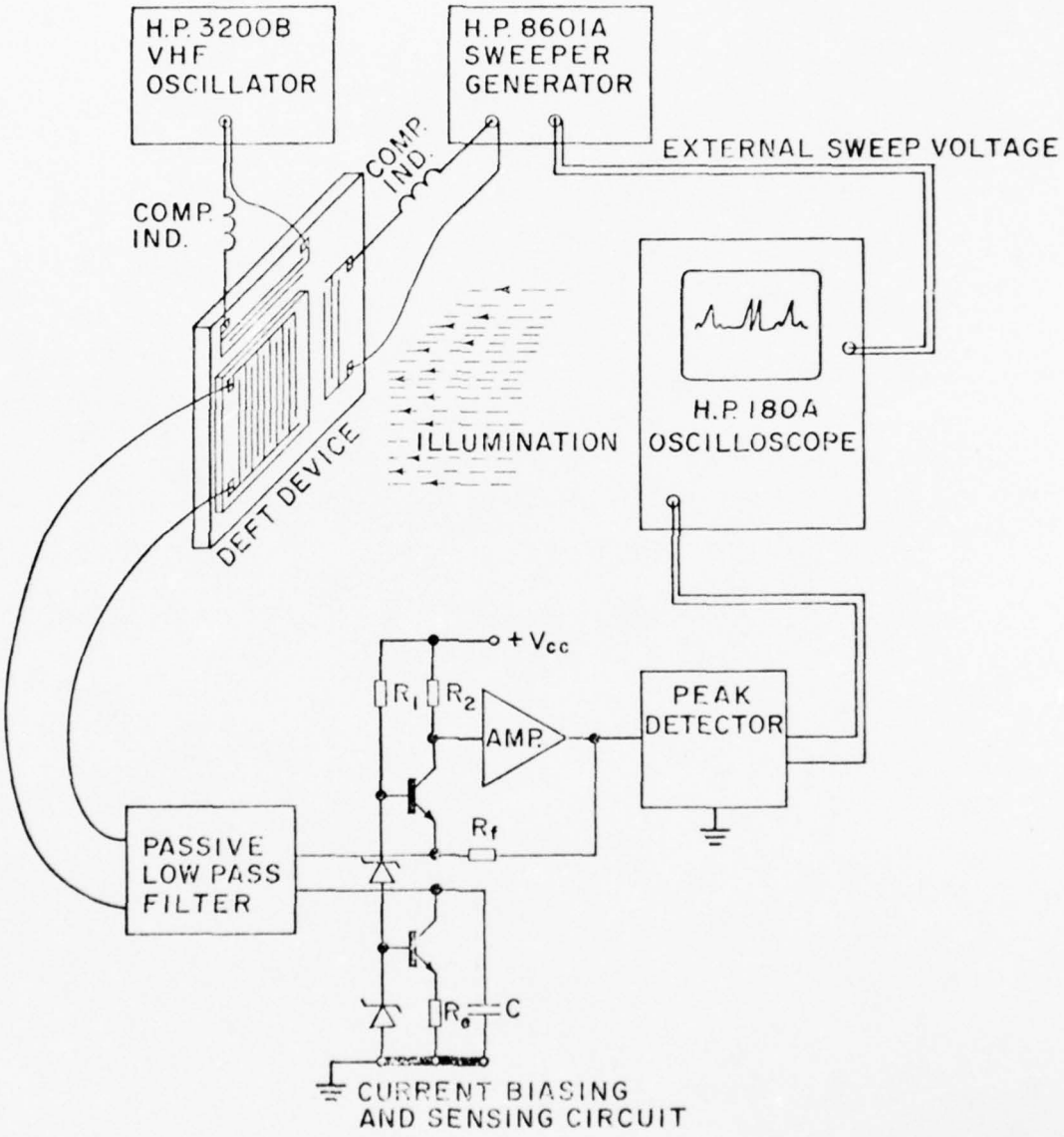

Fig. 2.4.3. Test Set-Up for the Two-Dimensional Sensor. Note the compensating inductors for each transducer.

We also were able to make phase measurements verifying that the sensor satisfies the Fourier translation theorem along any arbitrary axis.

Again we used objects with only three components within the bandwidth of the system. The projected gratings, with periodicities of between two and four millimeters, have their zero spatial frequency components in the middle of the reduced space while their fundamental frequencies were within the 4 MHz x 4 MHz reduced space. Harmonics mostly fell outside the reduced space scanned by the transducers.

Our first task was to map out the reduced space in terms of temporal frequencies. That is, we had to find out exactly what temporal frequency combination (ω_1, ω_2) corresponded to $g_x = g_y = 0$, the center of the reduced space. We also used to identify the temporal frequencies corresponding to the axes, $g_x = 0$ and $g_y = 0$. This we did by projecting a grid so that its spatial frequencies were along the g_x axis. By searching we found a line in temporal frequency space (f_2 = 30.15 MHz, 26.63 MHz < f_1 < 30.93 MHz) along which we observed the two symmetric fundamental lobes, plus a large central peak. Other lines would at most have one peak. Similarly, by rotating the grid 90°, we were able to find the useful g_y axis corresponding to (f_1 = 28.72 MH_3, 27.6 MHz < f_2 < 31.5 MHz). Thus the center of frequency space corresponds to (28.72 MHz, 30.15 MHz). From this point on, we can extrapolate to find any point in the reduced space.

By using the grid in the two different orthogonal orientations, we can calculate the velocities of the two surface acoustic waves. Knowing the value of g_i, the spatial frequency, obtained by ruler, we can

determine the experimental values ω_1 and ω_2 at which the fundamental appears for the two orientations. Then

$$g_i = \frac{\omega_1}{2\pi v_x} = \frac{\omega_2}{2\pi v_y} \tag{2.4.4}$$

where v_x and v_y are the phase velocities of the two acoustic waves. Thus we obtain

$$\frac{\omega_1}{\omega_2} = \frac{v_x}{v_y} = \frac{26.63 \text{ MHz}}{26.96 \text{ MHz}} = 0.988 \tag{2.4.5}$$

for the ratio of the velocities, using the actual frequencies.

The next stage in these experiments was to electronically rotate the spatial frequency space. Starting out along the y-axis, we rotated the grid in 10° steps, which was sufficient to completely eliminate the signal. While continuing to scan in one direction, the constant frequency source is readjusted to recapture the signal as shown in Fig. 2.4.4. Each trace, corresponding to one 10° step with the appropriate readjustment, represents a straight line in frequency space. As can readily be seen, the peak moves "in" toward the axis orthogonal to its original orientation. That is the projection of the spatial frequency vector starts out parallel to the scanning dimension and is then rotated away. Note that the zero frequency peak disappears after several scans since it remains centered on the original scan line. It will reappear as the rotation nears 180°. Each trace represents a horizontal line in frequency space, each with a different ω_2 intercept.

Fig. 2.4.5 shows the results of an identical experiment using a different grid. These peaks are the same width as in the previous figures as predicted by (2.1.19).

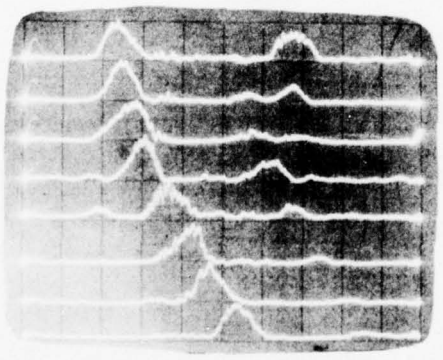

Fig. 2.4.4. The Magnitudes of Spatial Frequency Components Along Horizontal Axes in Fourier Space. Each trace shows the movement of a frequency component under successive 10° rotation of the image.

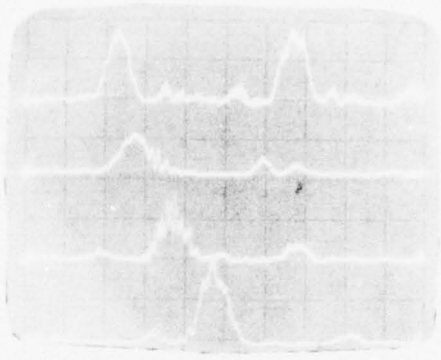

Fig. 2.4.5. The Magnitudes of Spatial Frequency Components for a Different Grid Object.

Experiments of this type were carried out over an entire 360° rotation. It was possible to track a spatial frequency component throughout. Furthermore, it was usually possible to find both non-zero fundamental frequency components. Table 2.1 shows typical data from such an experiment. Here, after each rotation, the principal three components were reacquired by changing one frequency, and scanning along the other. In each case, the zero frequency peak was checked and the other fundamental lobe was found also. As the data shows, a rotation of the image away from the y-axis is compensated for by decreasing f_1 and increasing f_2 for the third quadrant fundamental peak (A), and by increasing f_1 and decreasing f_2 in the first quadrant peak (B). The zero frequency peak remains virtually unchanged as expected.

	A			B			Zero Spatial Frequency		
θ degrees	f_1 MHz	f_2 MHz	ampl. mV.	f_1 MHz	f_2 MHz	ampl. mV.	f_1 MHz	f_2 MHz	ampl. mV.
2.5	28.72	26.96	150	28.72	30.86	50	28.7	29.26	200
12.5	28.27	27.11	250	29.31	31.36	150	28.76	29.26	235
22.5	27.87	27.16	200	29.62	31.16	150	28.77	29.26	230
32.5	27.68	27.26	200	29.87	31.16	150	28.76	29.26	250
52.5	27.03	27.96	390	30.42	30.66	50	28.75	29.26	250
62.5	26.89	28.26	390	30.64	28.26	160	28.77	29.26	200

Table 2.1 Pseudo Beam Steering Experiment. For each rotation, the spatial frequencies of all three prominent components are given and their amplitudes noted. θ is measured from the y-axis. Amplitudes are at the detector output.

These results are strong evidence for the pseudo beam steering effect. Indeed, the very fact of obtaining these signals at all is strong evidence since the existence of signals depends on the vector addition of the wavevectors in order for the image transform space and the acoustic-space to be superimposed.

It will be noticed that the data points have some quantitative discrepancies. Components A and B do not have the same amplitudes, and the frequencies do not vary uniformly from one point to the next. We believe that this is due to very strong nonuniformities in the acoustic fields. In this sensor, apodized transducers are used. These transducers have a highly non-uniform amplitude over the wavefront, since some finger pairs only generate acoustic waves near the center line, while others generate across the entire wavefront.

There are alternative designs, however. We could employ multistrip couplers to create uniform wavefronts, or we could use a simpler transducer with more gradual fall off at band edge, but unapodized. We have chosen the second approach for the time being.

To perform phase measurements, the set up of Fig. 2.4.3 needs to be modified. Since the difference frequency is generated in the CdS film, there is no reference against which the signal phase can be measured. Therefore, a reference must be created electronically by mixing signals from the same generators that drive the transducers. Fig. 2.4.6 shows the test set-up devised for this purpose. Naturally, absolute phase is not particularly useful at this stage, but relative phase is of great interest. Specifically, we want to determine if the device operates consistently with the Fourier translation theorem. Thus we want to measure

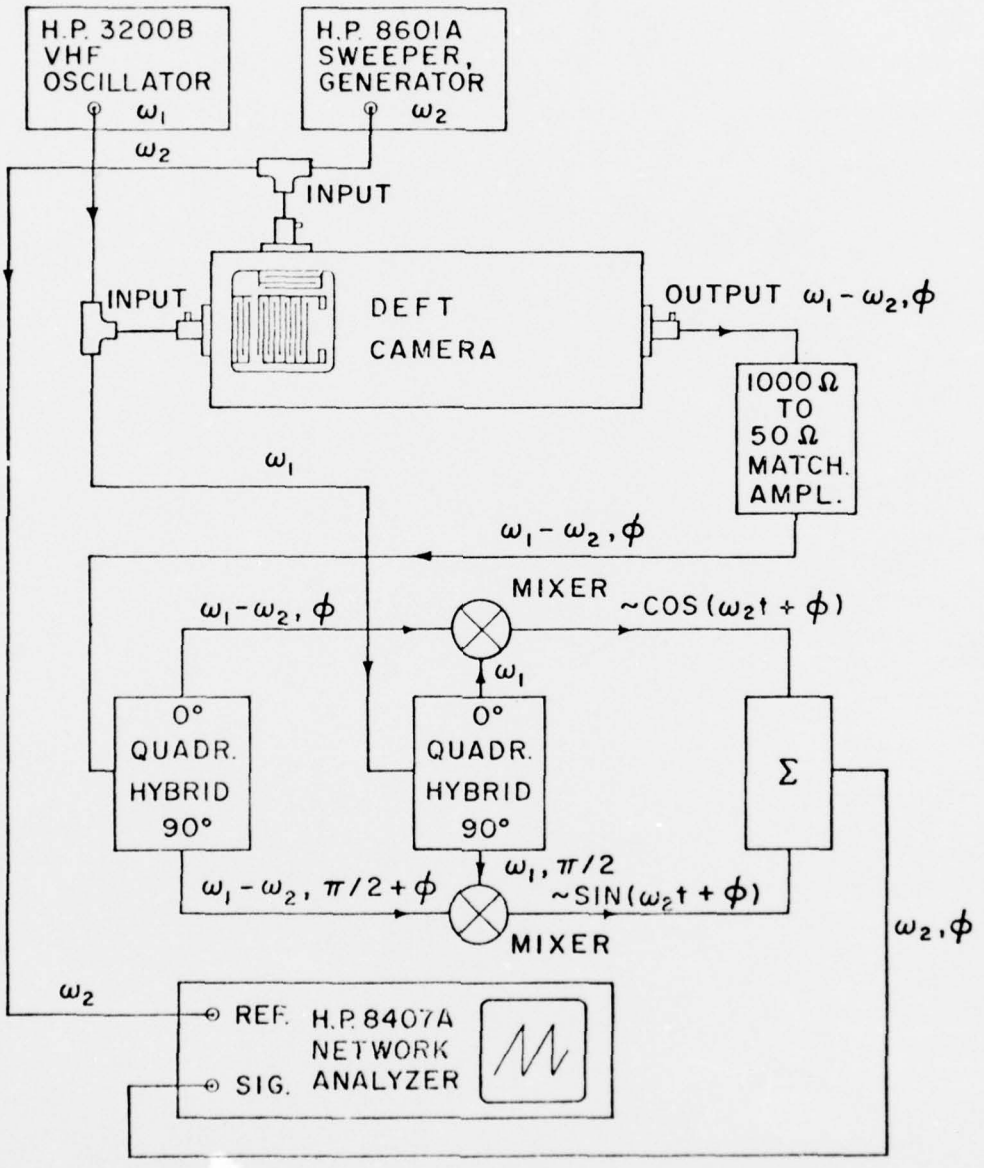

Fig. 2.4.6. Phase Detection System. The mixer together with the quadrative hybrids create the reference signals which the HP Network Analyser can compare to the DEFT sensor output.

the change of phase of a given spatial frequency component as a function of image displacement. These measurements were made successfully for the glass substrate sensors using the linear change of photoconductivity with strain and formed the basis for the motion-detection application.[6]

Qualitative measurements resulting from our set up were most encouraging. Fig. 2.4.7 reveals the linear variation of phase with frequency for a stationary grid image pattern. As can be readily seen, the phase is linear in the region of the peak, and deteriorates off the peak since there is really no signal being detected. As the image is displaced in any direction, the straight line sweeps across the peak region, while the peaks remains stationary, save for some minor changes in detail.

This is quite consistent with the Fourier translation theorem,

$$I_i(\vec{r} - \vec{r}_0) \leftrightarrow I(\vec{f}) \exp -j2\pi[\vec{f} \cdot \vec{r}_0] \tag{2.4.6}$$

where $\vec{f} = f_x\hat{x} + f_y\hat{y}$.

More generally, from (2.1.19)

$$I_i(\vec{r} - \vec{r}_0)\ S(\vec{r})\ A(\vec{r}) \leftrightarrow \bar{I}(\vec{g}) \exp -j2\pi[\vec{g} \cdot \vec{r}_0] \tag{2.4.7}$$

where $\vec{g} = g_x\hat{x} + g_y\hat{y}$, the reduced vector spatial frequency, and $\bar{I}$ is the smoothed version of I.

Thus we expect a linear change in phase,

$$\Phi = -2\pi\ \vec{g} \cdot \vec{r}_0 \tag{2.4.8}$$

for a displacement of the image $\vec{r}_0$. This implies that in order to tell the direction and distance involved in the displacement, two measurements of Φ must be made, although only one spatial frequency is needed.

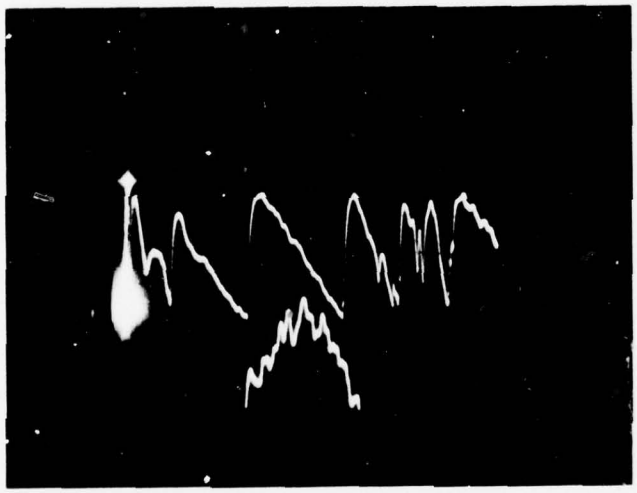

Fig. 2.4.7. Phase and Amplitude versus Frequency. With one frequency fixed, we see the amplitude and phase as a function of the scanning frequency near a peak. Phase is shown in the upper trace, amplitude in the lower.

We set out to check (2.4.8) quantitatively as well. After adjusting the image so that its fundamental spatial frequency vector $\vec{g}_i$ is along a particular direction, measured by protractor from the object itself, we translated the image, using precision micrometer translation stages, in the x-direction and the y-direction until we had measured some specific phase change.

From (2.4.8)

$$\Phi_x = -2\pi |g_i| \Delta x \cos\theta \tag{2.4.9}$$

for motion along the x-axis, Δx, where θ is the smallest angle between $\vec{g}_i$ and the x-axis.

Similarly for translation along the y-axis,

$$\Phi_y = -2\pi |g_i| \Delta y \sin\theta \, . \tag{2.4.10}$$

As one additional check, suppose that we choose $\Phi_x = \Phi_y$, then

$$\frac{\Delta y}{\Delta x} = \text{cotan}\,\theta \tag{2.4.11}$$

Table 2.2 shows data for this case, $\Phi_x = \Phi_y = 2\pi$, a particularly easy phase to measure of the HP Network Analyser. The results from (2.4.9), (2.4.10), and (2.4.11) yield the correct orientation for the pattern to within 10%. This is a very strong quantitative test of pseudo beam steering, and therefore, of Fourier imaging.

Δy measured	Δx measured	θ (2.4.10)	θ (2.4.9)	θ (2.4.11)	θ measured
.0659"	.0761"	45.8°	51.6°	49°	47°

TABLE 2.2. Quantitative measurement of angle from phase measurements. Here $|g_i| = 833.3\ m^{-1}$, a period of 1.2 mm.

II.4.3. Conclusions

We have successfully fabricated a monolithic, two-dimensional acoustooptical processor, yielding real-time Fourier transform magnitude and phase data. This is a significant breakthrough. As we will discuss in Section V, this technology may have benefits considerably beyond the confines of the applications already demonstrated, and even envisioned, for Fourier image processing systems. The magnitude of the acoustically-induced modulation is so large that convolvers and correlators, including memory, may be fashioned using CdS on $LiNbO_3$, using either a one- or two-dimensional geometry.

The fact that the effect is so profound (20% modulation of the photoconductivity), coupled with our success in making stable, highly photoconductive films of CdS on z-cut $LiNbO_3$, implies that we can concentrate our efforts on improvements. We are striving now to improve film uniformity, since the current films have photoconductivity variations of 50% over the surface. Evidence leads us to believe this problem is centered in the curing stage, caused by non-uniform gas flow in the diffusion furnace.

Improvement in transducer design is also a high priority aimed at developing a more uniform,collimated wavefront.

Electronic design to incorporate drivers and detection electronics is also of great interest in order to make the "sensor" into a "camera".

Fig. 2.4.8 shows the extent to which this has been accomplished. The sensor is roughly the size of a penny, while the entire system (sensor, detection electronics) is contained in a box 25 cm. x 6 cm. x 2.5 cm., containing five transistors and about thirty passive elements.

Fig. 2.4.8a. The Sensor (CdS, contacts, transducers, on $LiNbO_3$). Note the size relation to a U.S. one cent piece.

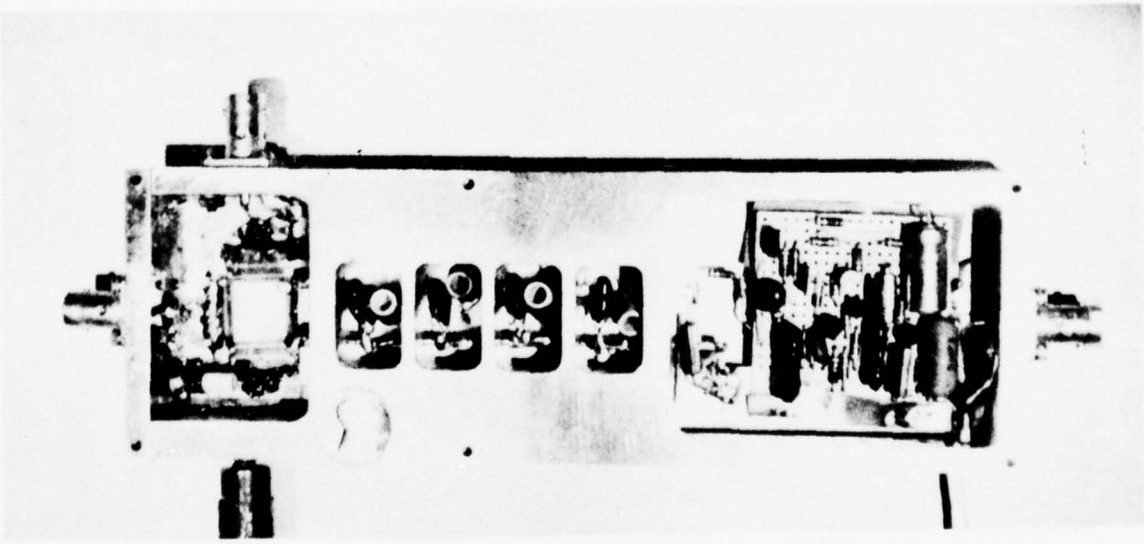

Fig. 3.4.8.b. The Camera. On the left is the cavity containing the sensor and the inductors used for tuning the transducers. The central four cavities hold the detection filter.. The right cavity holds the biasing and amplifying circuits.

III. DEFT LIGHT VALVE

A considerable effort was expended to fabricate a two-dimensional DEFT light valve. Such a system is shown in Appendix I which includes a description of its basic principles of operation. This device relies on strain-induced birefringence in a light valve sandwich. The image is focussed on the surface of a $LiNbO_3$ crystal. This device is very similar operationally and schematically to the electrophotoconductive device except that the interaction region has no CdS and no contacts. This is due to the fact that the intensity modulation has a component proportional to the strain squared. The modulated light passes through the polarizer-valve-analyzer sandwich and is detected by our E.G. + G. high sensitivity spectroradiometer with circuitry tuned to the difference frequency. This structure requires more light but is easier to build, at least for use as an optical instrument, since it is made from existing hardware. It will also not suffer from relaxation time effects, thus providing much faster time response to image changes. It should also provide more spatially uniform processing.

Such a system was built and assembled on our optical table. At present, no useful data has been obtained because the $LiNbO_3$ crystal appears to have a very non-uniform internal birefringence. Theoretical work indicates such natural birefrengence should be very small, but would not be too serious even if it exists. Unfortunately, this effect is quite non-uniform over the active area of the device. Thus the polarizers are unable to cancel out this natural birefringence, causing a complex pattern of light to exit the sandwich. This amount of light is too great to allow the detection of the signal since it induces a photocurrent in the highly sensitive detector of approximately 10^{-7} amperes. Although this effect is essentially d.c., it creates a large noise signal

in the detector because it is driven close to saturation. The signals we are searching for were calculated to be in the range of 10^{-9} amperes and thus are completely lost in the noise.

Our current effort is to build a bulk travelling wave device consisting of a highly polished, optically flat, fused quartz slab with $LiNbO_3$ transducers professionally bonded. This system will work at center frequencies of 40 MHz with 15% bandwidth. Fused quartz is not naturally birefringent, thus eliminating our main difficulty. Also, by going to a bulk wave device, a much larger interaction length between the optical intensity and the crossed acoustic fields is provided. The bulk waves will be effectively absorbed by careful sandblasting of the edges of the quartz on opposites edges from the transducers. Thus we will have a travelling wave acoustic system. Standing waves are not desirable since the geometry of the crystal has a dominant effect on acoustic behavior, rather than the transducers.

IV. A DISCUSSION OF THE APPLICATION OF DEFT SPATIAL SPECTRAL ANALYZERS

IV. 1. Image Reconstruction from DEFT Spectra

A DEFT spectrum analyzer performs the function of Fourier analysis by interrogating the input image with acoustic waves of various spatial frequencies, in particular directions. An acoustic wave, launched in a given direction, with a particular spatial frequency, tests the image at one corresponding value in the two-dimensional $\vec{k}$-space. By measuring the spectrum in this manner at a number of points, the entire image spectrum can be sampled.

To reconstruct the image from this information, all the measured Fourier components have to be reassembled, with due regard to their relative phase values. In a two-dimensional spatial situation such as this, each frequency component can be viewed with phase exhibited as the proper translational position of the bars of the grating. The coherent addition of all these gratings reconstructs the original image.

The required Fourier process is provided by an optical lens between its front and back focal planes. If an image transform is offered to such a lens with the spectral components properly arranged in $\vec{k}$-space in the front focal plane, with coherent illumination, an image reconstruction will be found in the back focal plane. It is important to notice that all the spectral components are required to be available simultaneously at a given time for the coherent optical transformation to take place.

The DEFT device generates these components in serial fashion, and thus some storage medium between the DEFT forward transformer, and the optical inverse transformer is needed to handle DEFT data. This storage

mechanism can be an optical modulator in the front focal plane that stores input information long enough for all of the significant Fourier components to be tested by the DEFT device and loaded into the modulator.

The same storage requirement presents itself if a second DEFT device is to be used to provide the Fourier inversion. The spatial spectrum of the image must then be incident in optical form, arranged in $\vec{k}$-space, on the second DEFT, all simultaneously in time. Thus an optical modulator of some kind is still needed to sort and store the data in this way, and the second DEFT device is essentially a replacement for the lens in an optical reconstruction.

IV. 2. Incoherent Reconstruction

The use of an incoherent optical modulator, such as a CRT does not appear to produce a viable option. Such a light source does not provide the spatial phase coherence from point to point that is required when a lens is to be used as a coherent Fourier transformer. Each radiating point in the phosphor screen of a CRT is an independent source of light, and bears no relationship to the phase of the light emitted at any other point. The bandwidth of the radiation is large enough that the phase relationships completely change in a time much shorter than the minimum time resolution of any known detector. Thus the CRT, or its equivalent, does not satisfy the requirement that the various spectral values in $\vec{k}$-space be reassembled with the proper phase relationship in image reconstruction.

The question may arise if it is possible to perform optically incoherent reconstruction using a CRT, and an integrating medium, such as photographic film. The technique which is suggested to write a grating on the CRT for each measured spectral component from the DEFT device, in the form

of a black and white grating pattern, and exposing the photographic film to this pattern. The process would be repeated for each measured spectral component by the DEFT device. In this manner, each of the proper spatial frequencies present in the original image would be built up into a reconstruction.

The difficulty with this approach is the required bias level in each contributory grating. In coherent methods, each spatial frequency can be introduced without bias, i.e. the grating can be written with 0 bias, swinging positive and negative in value. In the incoherent methods, the grating cannot have a value less than 0 (black). Thus a large number of bias terms are added to the final reconstruction, which greatly reduces contrast, signal-to-noise ratio, and image quality.

IV. 3. Coherent Optical Reconstructors

There are a number of optical coherent area modulators in existence. The operation of these are based on 1) a mechanical deformation, 2) an electro-optical effect (usually the Pockel's effect), or 3) interaction between an acoustic wave and an optical beam. Competitive two-dimensional devices can achieve at least several hundred resolution elements along a side, up to 1000 elements. Most of them fall within a narrow size range, 1 to 3 cm. on a side.

Mechanical deformation can be induced by the electrical force associated with charge deposited on a deformable film; this is the case in the General Electric coherent light valve, where the active medium is a thin film of fluid that deforms according to the electron beam pattern produced on the surface of the fluid. The charge is deposited by an electron beam in a sealed tube, so that the device resembles a CRT with the oil film target as a replacement for the phosphor screen. A 2 cm. square

aperture is used presently for the active raster-formatted data. An increase in size would entail a major expense for the mechanical redesign of the sealed vacuum tube.

Also, there has been developed at Perkin-Elmer a membrane modulator in which mechanical deflection is provided by a thin membrane overcoated on a substrate, containing a matrix of holes, each one delineating a resolution cell of the modulator. The electric force can be provided directly by charge, or by combining the device with a photoconductor which responds to an input optical image.

Electro-optical effects in crystals are the basis of another class of modulators. A number of ferroelectric crystals exhibit a change in optical birefringence when subjected to an electric field. Birefringence refers to that quality of an optical medium in which there is a different amount of optical phase shift, or phase delay, through the medium for light polarized in different directions. Thus a crystal used as a Pockel's cell, phase-modulates a light beam passing through it as a function of the electrical excitation and, moreover, the amount of this phase modulation will be different for light polarized along the two orthogonally oriented principal axes of the crystal. It can be shown that if light polarized at an angle of 45° to these axes is modulated in this way, the linear polarization is converted to elliptical polarization by the birefringence of the crystal. If the resulting light is now analyzed by a polarizer oriented at right angles to the original polarization axis of the light, the final light beam obtained from the second polarizer will be amplitude-modulated by the action of the Pockel's cell. Thus both phase and amplitude optical modulation can be obtained.[1,17]

The Itek "PROM" (Pockel's Read-Out Optical Modulator) is an example of this technique. In the case of the PROM, the field pattern is created by an incident light pattern and a photoconductive effect in the crystal.

A similar device has been developed at Carnegie-Mellon University, which like the G.E. light valve, is written on with an electron beam. In this case the target is a Pockel's effect thin crystal, KDP.

Another important development is the use of a liquid crystal to realize a coherent modulator, such as has been fabricated at Hughes Research Labs., Malibu, Calif. The device makes use of a very thin layer of a liquid crystal that exhibits a particular molecular orientation depending on the local voltage applied across the film, which, in turn, is made to represent an input light pattern by the action of a photoconductive layer sandwiched between the liquid crystal layer. The photoconductive layer causes the excitation voltage to be modified in areas where light strikes it. In this respect, the device is operated much like the Itek "PROM".

The foregoing discussion has touched on the major types of coherent area modulators available, that have sufficient time storage to be a possible candidate for a Fourier inverter of DEFT information. The G.E. light valve, and the KDP light valve have the advantage of using input electronic data directly, which is the form of the DEFT output. The PROM and the Hughes' Liquid Crystal require an optical input, so that they must be paired with an optical projector, such as a CRT.

At the present time, all these modulators are in developmental stages, and single units cost in excess of $40,000. A complete Fourier inverter system using any of them is estimated to cost at least $100,000.

IV. 4. Conclusions Regarding DEFT Spatial Spectral Analyzers

In the above discussion, it is evident that there are complexities to be faced if it is desired to Fourier-invert electronic data from a DEFT device to recover an original image. From this impression, it is suspected that the most efficient utilization of a DEFT device is to use the Fourier components measured by the DEFT device from an image directly. Thus the recognition or classification of objects contained within an image on the basis of observed Fourier components would be a natural utilization of the DEFT with regard to the form of data which it provides.

It is thus felt that the most fruitful application studies for the DEFT would be in the area of image analysis using measured Fourier data. In many cases, the spatial shape of the Fourier presentation is a good indication of the real domain shape of the important features in a scene, and the Fourier information can also provide an indicator of the presence of some type of object of interest. The advantage of using the Fourier domain for this type of detection is that the Fourier intensity pattern does not translate its position as the object translates. Thus is may be considerably easier to search the Fourier plane for automatic feature recognition than the real plane itself. Examples may be pointed out: patterns with strong repetition produce strong impulses or bright spots in the Fourier plane; triangular structures produce a star-like pattern with a hexagonal characteristic in the Fourier plane; circular objects produce circular transforms.

This type of Fourier recognition analysis should be the subject of a separate study, in which the concepts are experimentally tested.

V. FUTURE WORK

V.1. Near Term Efforts

Currently, we are pursuing the work mandated by the contract. We have not encountered any dead ends, and indeed are very encouraged by important successes accomplished this year. Having fabricated good films of CdS on $LiNbO_3$ and found that they possess a truly remarkable acoustic modulation of the photoconductivity (20%), we feel confident that no significant problem bars the way to useful applications for the DEFT technology.

As discussed in Section II, current efforts are to improve the curing process in order to obtain greater uniformity, larger light-to-dark conductivity ratios, and cleaner surfaces. Extensive studies of ultimate sensitivity and carrier lifetimes are currently under way.

We are also evaluating two methods of producing etched CdS films. One method is to etch out squares of CdS rather than lines. Thus the indium/aluminum contacts will not have to go up and down over the CdS, but merely touch the edges. The other method is to make the metal thicker so that it won't break.

Since the CdS films turned out to be so thin, we will endeavor to increase the evaporation time to increase their thickness by at least a factor of five. This will increase the sheet conductivity by the same factor, but will make etching somewhat harder as well.

One problem currently being addressed is the nonuniformity of the acoustic wavefronts. It is quite evident that apodized transducers are not well suited for a two-dimensional sensor, although they may be adequate for a unidirectional version. The smoother, more symmetric behavior

of the unidirectional sensor can be observed in the data of Section II, and appears directly related to the acoustics.

We are preparing to test new sensors with an unapodized design. These tests should clearly establish the degree to which further inprovement of acoustics is needed.

By introducing further spacings between transducers and the CdS film contact region, we hope to operate devices in the gated mode, making possible spatial raster scanning sensors in addition to Fourier imaging sensors with very low spurious signal levels.

During the coming months, we will be interested to try some new materials to evaluate their promise in DEFT sensors. We expect to study the acoustic modulation in infrared sensitive films provided by NVL. It may be possible to fabricate either a device depending on the linear change of photoconductivity[1-7], or the quadratic effect in electric field discussed in this report. The quadratic effect is, of course, essential for full two-dimensional Fourier imaging.

CdSe is another material which might offer some advantages over CdS, including faster optical behavior. Single crystal films of CdS, now available, may also be useful, providing that we can learn how to cure them, or dope them by other means.

The work on light valve processors continues as well with the fabrication of a bulk travelling acoustic wave device of fused quartz described in Section III.

Based on the next month of work on improving the 30 MHz center frequency sensors, we will design and build a sensor in the 100 MHz range. Such a sensor will verge on a practical processor capable of yielding

over 1500 Fourier components.

As the sensors become practical, we must continue to develop fields of application. An ongoing effort is to study pattern recognition and reconstruction aspects of their use as an incentive to the more fundamental physical research. We intend to continue to investigate the area of signal design[1], aimed at obtaining other transform representations, in order to broaden the applications.

V.2. New Applications

New applications are now open to DEFT technology beyond those envisioned when the work under this contract was initiated. It is quite clear that we are now in a position to design and fabricate convolvers, correlators and amplifiers for electronic microwave signals. These three signal processing applications can be achieved through coupling between drifting carriers and acoustic waves.

Extensive research on these applications has led to a number of useful devices,[25-28] principally convolvers for radar processing.

Most convolvers and correlators presently being developed are based either on a nonlinear piezoelectric effect in a crystal such as $LiNbO_3$[26], or on the separated medium structure.[25, 27, 28] The separated medium structure consists of a $LiNbO_3$ substrate, with a Si bar supported over a piezoelectric substrate with an air gap in between. The nonlinear piezoelectric devices are simple, monolithic structures but have very small convolution signals due to the small nonlinearity. The separated medium devices have had the most success since they use the usual piezoelectric behavior of the substrate and a nonlinear coupling to the electrons in the Si bar. Unfortunately, practical versions of this device are very difficult to construct because a uniform 1000Å air gap must be maintained between the $LiNbO_3$ substrate and the Si bar.[28]

A very promising structure is the monolithic conducting thin film on a piezoelectric substrate. Luukkala[11] has described a $CdSe/LiNbO_3$ imaging convolver and Solie[27] has described a $CdSe/LiNbO_3$ amplifing convolver. With our technology, we could make a $CdS/LiNbO_3$ device for

either purpose, depending on the curing procedure and on the pick-up contact pattern design. With additional support, these applications could be evaluated rather readily. We have every reason to expect that our films are as satisfactory and reproducible as those presently used in convolvers.

All of the work discussed in this section so far is concerned with unidirectioned, one-dimensional, signal processing. The newest frontier in SAW processing is the memory convolver.[29, 30] Here the Si bar is made into a linear array of either p-n diodes or charge coupled devices (CCD).[31] In such structures, the SAW can interact with a stored electronic signal. In the CCD, the SAW could also serve as the "clocking electrodes" in the usual CCD, by storing the charge in wells created by the SAW electric fields.

The maximum utility of this approach would be for a two-dimensional array of diodes or CCDs. At present, the only suggestions for accomplishing this have relied on many lines each with its own transducers.

Our proposal is to make CdS CCDs on the z-cut $LiNbO_3$ surface, thus producing a monolithic structure. Fig. 5.2.1 shows the schematic structure of one line of such an array. In the dark, the charge could be injected at one end and clocked along. Alternatively, the signal could be read in optically. This structure might have advantages over Si devices due to the fact that in the dark CdS is a much better insulator than Si yielding higher transfer efficiency.

With the addition of acoustic transducers and collecting electrodes we can now modulate the stored charge with the acoustic waves. Consider a SAW-CCD convolver shown in Fig. 5.2.2. This device consists of a double

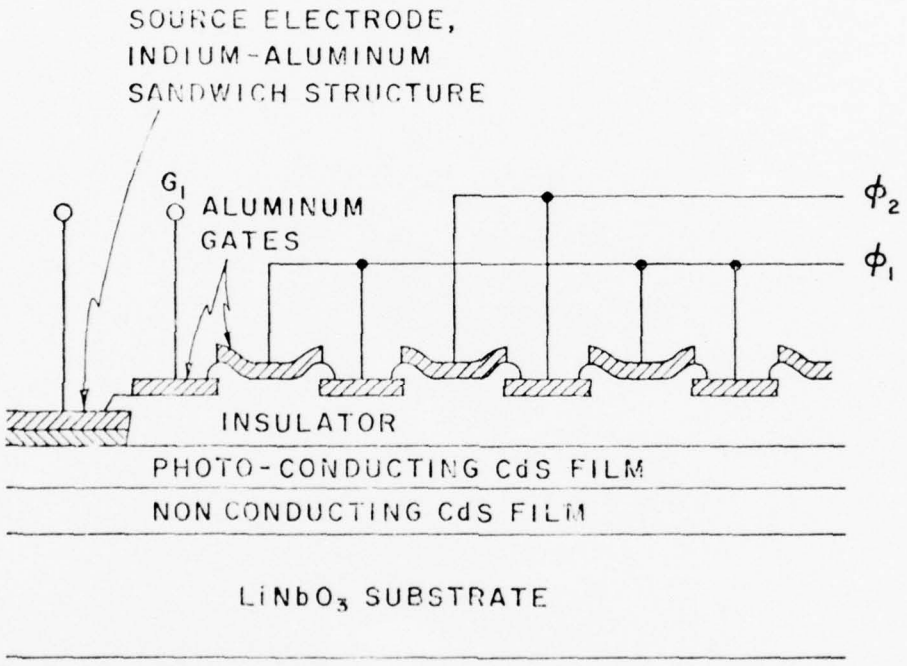

Fig. 5.2.1. Schematic of a CdS array of Charge Controlled Devices. It is shown on $LiNbO_3$ but could easily be made on glass or fused quartz.

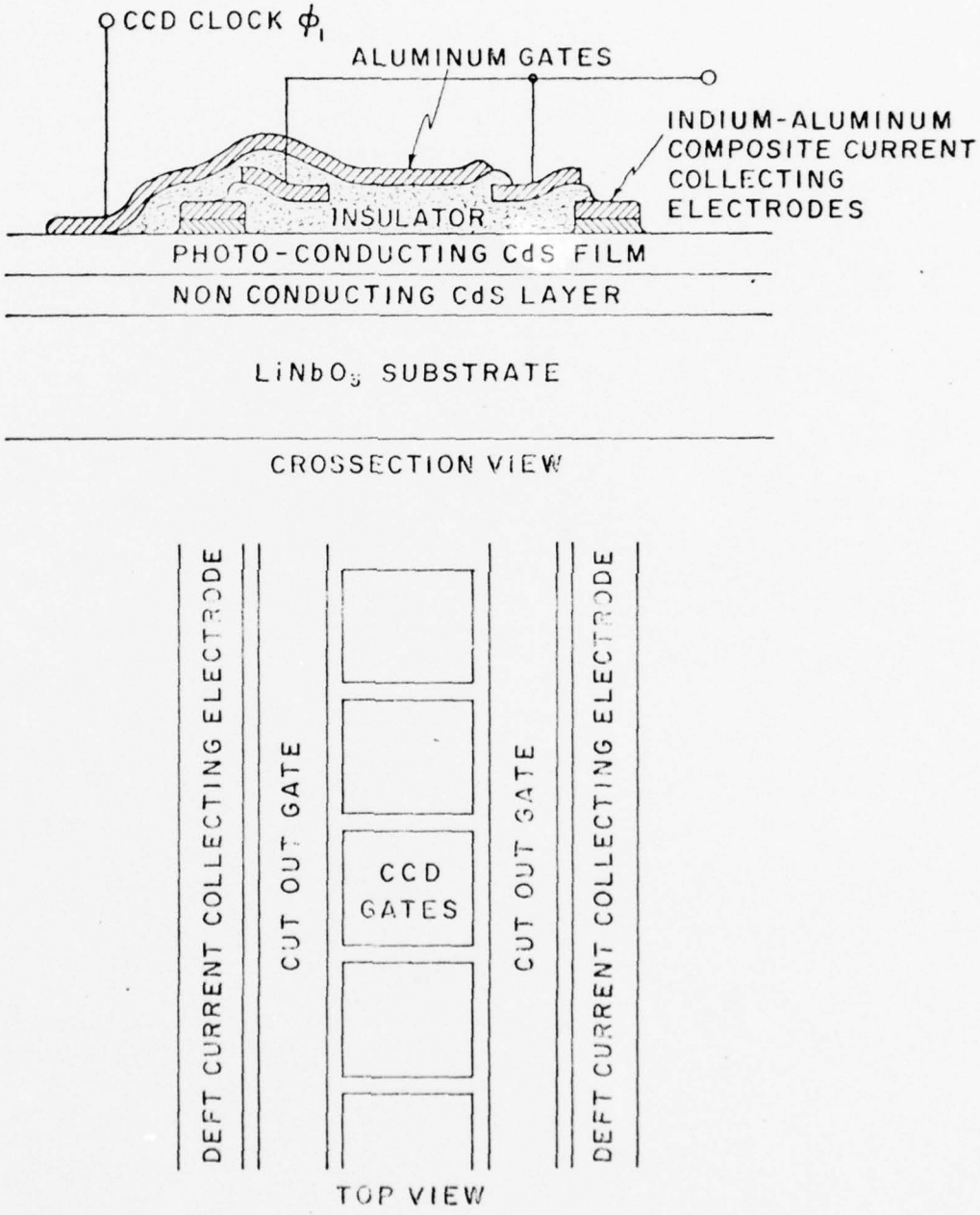

Fig. 5.2.2. Schematic of a SAW-CCD Memory Convolver Structure. The cut-out gates provide the lock-out feature described in the text.

layer CdS film fabricated on a z-cut $LiNbO_3$ substrate. There are two current collecting contacts on each side of the device shown. A standard CCD is located between these contacts. To prevent the stored charge from being shorted while the CCD is being loaded it is necessary to isolate the CCD from the collecting electrodes. This is accomplished by potential barriers created by applying a sufficiently large negative voltage to the lock out gates.

The lock-out gates are activated by the application of a negative potential. This generates a potential barrier between the CCD and the current collecting electrodes. Next, the CCD is loaded in the conventional manner by clocking its gates. After the loading process is completed, the trap states are allowed to fill. This process takes about 1 ms. Next the potential barriers between the CCD and the collecting electrodes are lowered by the application of a small positive voltage to the lock-out gates. At the same time, a potential difference is established between the two current collecting electrodes. This is accomplished by the left electrode being grounded and applying a voltage to the right electrode. A short but large current pulse lasting about 20 nS will occur across the electrodes. This current pulse results from the mobile charge in the CCD charge packets being emptied. At this point in time, a SAW having an envelope function $f(t - x/v_s)$ and an angular frequency ω_1 and a second constant amplitude SAW of angular frequency ω_2 are launched colinearily, both in the same direction. The SAWs propagate along the CCD with wave fronts perpendicular to the electrodes.

The trapped charge will now trickle out. The current resulting from this trapped charge will behave essentially similar to the photocurrent modulated by the electric field associated with the SAWs in a way similar to the previously described. We are now interested in detecting the current component oscillating at the sum frequency $\omega_1 + \omega_2$ from each CCD section. The surface current density component K_n resulting from the n-th CCD charge packet and oscillating at the sum frequency will be proportional to

$$K_n \propto (q_n/\tau) f(t - na/v_s) \exp j(\omega_1 + \omega_2) na/v_s \tag{5.2.1}$$

where q_n is the trapped charge, τ is the relaxation time associated with emptying of the traps, v_s is the SAW velocity, and a is the periodicity of the CCD. Let us choose the angular frequencies in such a way that

$$(\omega_1 + \omega_2)/v_s = 2\pi/a. \tag{5.2.2}$$

The surface current density component of interest due to the trapped charge reduces to

$$K_n \propto (q_n/\tau) f(t - na/v_s). \tag{5.2.3}$$

The total collected current oscillating at the sum frequency i_{sig} is the sum of all the individual currents of all the CCD sections

$$i_{sig} = \sum_{n=1}^{N} K_n.$$

Thus

$$i_{sig} \propto \sum_{n=1}^{N} (q_n/\tau) f(t - na/v_s). \tag{5.2.4}$$

The total collected signal current component oscillating at the sum frequencies of the two SAWs is proportional to the discrete convolution of the trapped charge distribution q_n and the envelope of one of the SAW signals. The other SAW amplitude is maintained constant during this time period.

It would be advisable to operate a number of CCDs in parallel in order to increase the signal current. The signal current of such a device should be comparable to the signal current from our present image activated DEFT devices, typically 10 to 20 μA.

Of course, much work would be required, first to perfect the CdS CCD and then to fabricate a memory convolver. Until now, no one has been able to make adequate films of CdS. Once applied this technology is quite adaptable to the memory convolver two-dimensional array. The separated medium convolver may be very difficult to reproduce since the air gap must be maintained over a large area.

The high dark resistivity, high light conductivity, and extremely large acoustic modulation, make these new applications very tempting. If such devices could be developed, they would have a profound impact on signal processing and might be superior to those avenues already being explored.

Using the DEFT technology, these memory convolvers can be operated with several large transducers, relying on pseudo beam steering, rather than on a multitude of small, highly diffracting transducers operated by a complex switching system. The pseudo beam steering transducers can single out a given line of CCD devices by varying the relative delay of the driving signals.

Section VI

BIBLIOGRAPHY

1. P. G. Kornreich, S. T. Kowel, D. J. Fleming, N. T. Yang, A. Gupta, and O. Lewis, "DEFT: Direct Electronic Fourier Transforms of Optical Images," IEEE Proceedings, Vol. 62, pp. 1072-1087, August, 1974.

2. U. S. Patent #3,836,712 (9/17974).

3. S. T. Kowel, P. G. Kornreich, O. Lewis, A. Gupta, N. T. Yang, and R. Zawada, "DEFT: Progress on Direct Electronic Fourier Transforms of Two-Dimensional Images," RADC-TR-244, September 1974.

4. S. T. Kowel, P. G. Kornreich, O. Lewis, A. Gupta, and R. Zawada, "Progress on Two-Dimensional Direct Electronic Fourier Transform (DEFT) Devices," 1974 Ultrasonics Symposium Proceedings, pp. 763-767.

5. P. Kornreich, N. T. Yang, and S. T. Kowel, "A Direct Electronic Fourier Transform Device for Imaging," IEEE Proc. Letters, Vol., 61, August 1973.

6. S. T. Kowel, P. G. Kornreich, O. Lewis, and F. D. Kirschner, "Passive Detection of Motion Transverse to the Optical Viewing Axis," IEEE Trans. on Instrumentation and Measurement, Vol. IM-24, pp. 248-255, Sept. 1975.

7. S. T. Kowel, P. G. Kornreich, and O. Lewis, "Focus Detection Using Direct Electronic Fourier Transform Sensors," J. of Appl. Photographic Engineering, Vol. 2, #3, pp. 113-118, Summer 1976.

8. S. T. Kowel, P. G. Kornreich, A. Mahapatra, D. Cleverly, B. Emmer, and R. Zawada, "Two-Dimensional Fourier Imaging of Light Using Acoustic Pseudo-Beam Steering," 1975 Ultrasonics Symposium Proceedings, pp. 136-140. (Provided in Appendix A.)

9. S. T. Kowel, P. G. Kornreich, A. Mahapatra, and B. Emmer, "Experimental Confirmation of Two-Dimensional Acoustic Processing of Images," 1976 Ultrasonics Symposium Processing of Images," 1976 Ultrasonics Symposium Proceedings, pp. 668-672. (Provided in Appendix B.)

10. H. Gautier, G. S. Kino, and H. J. Shaw, "Acoustic Transform Techniques Applied to Optical Imaging," 1974 Ultrasonics Symposium Proceedings, pp. 99-103.

11. M. Luukkala, P. Merilainen, and K. Saarinen, "Acousto-Resistive Effects in Thin Film CdSe/$LiNbO_3$ Delay Line System," 1974 Ultrasonics Symposium Proceedings, pp. 345-348.

12. V. L. Newhouse, C. L. Chen, and K. L. Davis, "Possibility of Switching and Steering Surface Waves by Nonlinear Mixing in Anisotropic Media," J. Appl. Phys., Vol. 43, pp. 2603-2608, June 1972.

13. W. Franz, Zeitschrift Fur Naturforschung, Vol. 13a, p. 484 (1958).

14. L. V. Keldysh, Sh. Exsperim. i Teor. Fiz., Vol. 34, p. 1138 (1958); English Translation Sov. Phys. JETP, Vol. 7, p. 788 (1958).

15. E. S. Kohn and M. Lampert, Phys. Rev., Vol. B4, pp. 4479-4491, 1971.

16. J. F. Nye, Physical Properties of Crystals, Oxford, 1969.

17. A. Gupta, Ph.D. Dissertation, Syracuse University, 1975.

18. A. Waxman, V. Henreich, F. Schellcross, H. Borhan, P. Weimer, J. Appl. Phys., Vol. 36, p. 168 (1965).

19. M. Luukkala, private communication.

20. J. W. Goodman, Fourier Optics, McGraw-Hill, 1968.

21. J. M. Ziman, Principles of the Theory of Solids, Cambridge, 1965.

22. F. A. Jenkins and H. E. White, Fundamentals of Optics, 2nd Ed., McGraw-Hill, 1976.

23. H. I. Smith, F. J. Bachmer, and N. Efremow,"A High Yield Photolithographic Technique for Surface Wave Devices", J. of the Electrochemical Soc., Vol. 118, pp. 821-825, May 1971.

24. A. J. Slobodnik, Jr., E. D. Conway, and R. T. Delmonico, Microwave Acoustics Handbook, Air Force Cambridge Research Laboratories, 1973.

25. G. S. Kino, "Acoustoelectric Interactions in Acoustic-Surface-Wave Devices", Proc. IEEE, Vol. 64, May 1976, pp. 724-748.

26. P. Defranould and C. Maerfeld, "A Planar Piezoelectric Convolver", Proc. IEEE, Vol. 64, May 1976, pp. 748-751.

27. L. P. Solie, "A New Mode of Operation for the Surface-Wave Convolver", Proc. IEEE, Vol. 64, May 1976, pp. 760-763.

28. S. A. Reible, J. H. Cafarella, R. W. Ralston, and E. Stern, "Convolvers for DPSK Demodulation of Spread-Spectrum Signals", 1976 Ultrasonics Symposium Proc., pp. 451-455.

29. R. J. Schwartz, S. D. Goalema, and R. L. Gunshor, "Surface Wave Interaction Charge Coupled Devices, 1976 Ultrasonics Symposium Proc., pp. 197-200.

30. P. Defranould, H. Gautier, C. Maerfeld, and P. Tournois, "P-N Diode Memory Correlator", 1976 Ultrasonics Symposium Proc., pp. 336-347.

31. G. F. Amelio, W. J. Bertram, Jr., and M. F. Tompsett, IEEE Trans. on Electron Devices, Vol. ED18, pp. 986-992, Nov. 1971.

APPENDIX A

TWO DIMENSIONAL-FOURIER IMAGING OF LIGHT USING ACOUSTIC PSEUDO BEAM STEERING*

Stephen T. Kowel, Philipp G. Kornreich, Amaresh Mahapatra,
Dennis Cleverly, Bruce Emmer, and Robert Zawada
Department of Electrical and Computer Engineering
Syracuse University
Syracuse, New York 13210

* 1975 Ultrasonics Symposium Proceedings
IEEE Cat. #75 CHO 994-4SU

TWO-DIMENSIONAL FOURIER IMAGING OF LIGHT USING ACOUSTIC PSEUDO BEAM STEERING

Stephen T. Kowel, Philipp G. Kornreich, Amaresh Mahapatra,
Dennis Cleverly, Bruce Emmer, and Robert Zawada
Department of Electrical and Computer Engineering
Syracuse University
Syracuse, New York 13210

ABSTRACT. A new direct electronic Fourier transform (DEFT) system has been developed for two-dimensional imaging of two-dimensional signals. The image is focused on a birefringent crystal surface (e.g. $LiNbO_3$) on which two perpendicular SAWs are travelling, one at frequency ω_1, the other at ω_2. The birefringence created by the surface waves produces an effect proportional to the square of the sine of the local strain. This valve, placed between two crossed polarizers to block unmodulated light, yields an exit intensity of light containing a component proportional to the product of the input intensity with a sine wave "travelling" at the difference frequency and with an associated wavevector equal to the sum of the original wavevectors. Thus when this light is collected by a photocell, there is a term in the photocurrent at the difference frequency proportional to the $\bar{k}$ Fourier component of $I(\bar{r})$, where $\bar{k} = k_x\hat{x} + k_y\hat{y}$, is the vector sum created by the squaring effect of the birefringence, and $I(\bar{r})$ is the input optical signal. Thus by varying the transducer frequencies, arbitrary Fourier components can be obtained by this "pseudo beam steering", as if a new SAW had been created, but without the attendant difficulties.

Alternatively, an electrophotoconductive film (e.g. CdS) together with an interdigital contact can be deposited at the image plane in place of polarizers and photodetector. Here the a.c. current is derived from integrating the product of light intensity and the square of the electric field created by the SAW in the piezoelectric substrate.

Introduction

Acoustical imaging of light intensity patterns has received considerable attention; first for point-by-point scanning, and more recently for Fourier imaging [1,2,3,4,5]. This paper describes a novel, fully electronic, approach to the problem of extracting arbitrary, two-dimensional Fourier components of images.

The use of surface acoustic waves to modulate photoelectrons to produce electronic signals representative of spatial Fourier components of the image offers unique advantages over other methods of Fourier imaging. Reasonable bandwidths are available and good signal-to-noise ratios can be obtained because the entire image contributes to each Fourier component. In point-by-point systems, resolution is limited by the requirement for pulse lengths of many wavelengths, and output is small due to weak electroacoustic coupling combined with small sampling area.

Careful study of all present options shows that charge coupled devices (CCD's) are likely to be far superior as spatial scanners, and optical transforming systems, although extremely powerful, are difficult to interface with electronic systems.

In order to take full advantage of SAW Fourier imaging, it is essential to be able to electronically select arbitrary, two-dimensional, Fourier components of arbitrary, two-dimensional images. Previous work has been largely confined to obtaining one-dimensional transforms of one-dimensional [5,6] or two-dimensional images [1,4]. Various techniques have been proposed [1,4] for achieving full two-dimensional capability, culminating in the development of the pseudo beam steering technique discussed here.

The direct electronic Fourier transform (DEFT) devices derive signals representative of Fourier components by acoustically modulating photoelectrons. In the electrophotoconductive device, two surface acoustic waves, travelling perpendicularly, cross the image, focused on a thin photoconductive film (CdS in the current model). It has been demonstrated that the absorption of light is strongly dependent on applied electric field, with the generated photocurrent having a component proportional to the square of the electric field [7]. We provide the electric fields by propagating the two crossed surface acoustic waves on a piezoelectric substrate ($LiNbO_3$) on which the CdS has been deposited. A full tensor treatment of the interaction reveals that the deposited contacts detect a current proportional to

$$i(t) \propto \iint dx\, dy\, E_z^2\,(x,y,t)\; I\,(x,y) \qquad (1)$$

where $I(x,y)$ is the image intensity, x and y are the coordinates on the film, and E_z is the electric field perpendicular to the plane.

Since

$$E_z = E_1 \cos\,(\omega_1 t - k_1 x) + E_2 \cos\,(\omega_2 t + k_2 y) \qquad (2)$$

where E_1, ω_1, k_1, refer to the x-directed acoustic wave, and E_2, ω_2, k_2, refer to the y-directed acoustic wave, E_z^2 contains a term of the form

$$E_{zd}^2 \propto E_1\, E_2 \cos\,[(\omega_1 - \omega_2)t - (k_1 x + k_2 y)]$$
$$= E_1\, E_2 \cos\,[(\omega_1 - \omega_2)t - \bar{k}\cdot\bar{r}]. \qquad (3)$$

By varying the driving frequencies, we can vary $\bar{k}$, yielding a signal term proportional to the two-dimensional Fourier transform,

$$i_s(t) \propto \exp\,[j(\omega_1 - \omega_2)t] \int d^2\bar{r}\; I(\bar{r}) \exp\,(-j\bar{k}\cdot\bar{r}) \qquad (4)$$

while the other terms from (1) can be ignored because they are at different frequencies. That is, the signal behaves as if a new acoustic wave has been created with wavevector equal to the sum of the excited wavevectors. Thus we call this effect "pseudo beam steering".

An alternative structure being investigated relies on strain-induced birefringence in a light valve sandwich. Fig. (2) shows a schematic of the system in which this valve is employed. The image is focused on the surface of a $LiNbO_3$ crystal. This device is very similar operationally and schematically to the device in Fig. (1) (except that the interaction region has no CdS and no contacts). This is due to the fact that the intensity modulation has a component proportional to the strain squared. The modulated light passes through the polarizer-valve-analyzer sandwich and is detected by a photocell with circuitry tuned to the difference frequency. This structure requires more light but is easier to build, at least for use as an optical instrument, since it is made from existing hardware. It will also not suffer from relaxation time effects, thus providing much faster time response to image changes. Simple one-dimensional experiments have already been reported [4] for a similar structure.

From theoretical considerations, it appears that pseudo beam steering is likely to be far superior to

Part of the work reported here was supported by the National Science Foundation.

other proposed techniques for accomplishing two-dimensional imaging. For example, the actual creation of a third surface wave from nonlinear mixing appears to be a much smaller and less controllable effect.

The paper concludes with a review of the progress made and the expected commercial applications of these devices in motion and focus detection, pattern recognition, and image processing and reconstruction.

The Electrophotoconductive Sensor

The image sensor consists of a CdS film deposited on a y cut $LiNbO_3$ substrate, as shown in Fig. (1). Thin film indium contacts, in the form of an interdigital pattern, are deposited onto the CdS film. This pattern facilitates the collection of the total photocurrent over the area of the CdS film. Indium is used as contact material. It is our experience that indium makes ohmic contact to CdS. Aluminum pads must then be deposited over the indium before wires can be bonded.

Besides providing electrical contact, the contacts also form a grating across the image. This, in effect, shifts the Fourier transform of the image along the k_y direction to higher spatial frequencies. This allows us to generate the Fourier transform of the image with SAW's with a limited band width. A similar effect is obtained along the k_x direction by etching the CdS into lines along the x direction. We use, for simplicity, gratings with equal dark and light spacings. Unfortunately, this type of grating only exposes 1/4 of the CdS film to the image. Larger film exposurers are possible by making the dark areas of the masks narrower.

Since the photoconductivity of CdS has a term that depends on the square of the electric field, it is possible to obtain a mixing of the electric fields due to the two acoustic waves travelling perpendicularly to each other. This effect provides the effective steering of the wavevector, k, of the transform.

Although the various electric field and strain effects may vary through the thickness of the CdS film, we shall assume all effects to be uniform. Thus, the $\alpha\beta$ component of the conductance per square can be expanded to first order in the light intensity $I(x,y)$ and in the component of the strain tensor $\Sigma_{\mu\nu}$, and to second order in the electric field components E_μ, due to the SAW in the piezoelectric $LiNbO_3$ substrate, to yield

$$\sigma_{\alpha\beta}(x,y) = \sigma^D_{\alpha\beta} + \alpha^D_{\alpha\beta\mu\nu}\,\Sigma_{\mu\nu} + \sigma^L_{\alpha\beta} I(x,y) + \sigma^{LS}_{\alpha\beta\mu\nu} I(x,y)\Sigma_{\mu\nu} + \sigma^{DF}_{\alpha\beta\mu}\,E_\mu + \sigma^{LF}_{\alpha\beta\mu} I(x,y) E_\mu + \sigma^{DE}_{\alpha\beta\mu\nu}\,E_\mu\,E_\nu + \sigma^{LE}_{\alpha\beta\mu\nu} I(x,y) E_\mu\,E_\nu \ldots \quad (5)$$

where summation over like Greek indices is implied. Here

- $\sigma^D_{\alpha\beta}$ is the dark conductance per square,
- $\sigma^{DS}_{\alpha\beta\mu\nu}$ is the change of the dark conductance per square with strain $\Sigma_{\mu\nu}$,
- $\sigma^L_{\alpha\beta}$ is the change of the conductance per square with light flux $I(x,y)$, the ordinary photoconductivity,
- $\sigma^{LS}_{\alpha\beta\mu\nu}$ is the change of the conductance per square with light and strain,
- $\sigma^{DF}_{\alpha\beta\mu}$ is the linear change of the conductance per square with electric field,
- $\sigma^{LF}_{\alpha\beta\mu}$ is the linear change of the conductance per square with light and electric field,
- $\sigma^{DE}_{\alpha\beta\mu\nu}$ is the change of the conductance per square to second order with the electric field, and
- $\sigma^{LE}_{\alpha\beta\mu\nu}$ is the change of the conductance per square to first order in the light intensity and second order in the electric field.

Our polycrystalline CdS films have essentially isotrophic symmetry. Therefore all 3rd rank tensors must be zero. This requires that $\sigma^{DF}_{\alpha\beta\mu}$ and $\sigma^{LF}_{\alpha\beta\mu}$ be zero. This also requires that ordinary photoconductivity be essentially a scalar, σ_L. The dark conductance is small compared to the photoconductance at reasonable light levels for good photoconductive CdS. This allows us to neglect the terms $\sigma^D_{\alpha\beta}$, $\sigma^{DS}_{\alpha\beta\mu\nu}$, and $\sigma^{DE}_{\alpha\beta\mu\nu}$. This reduces (5) to

$$\sigma_{\alpha\beta}(x,y) = \sigma_L\,\delta_{\alpha\beta}\,I(x,y) + \sigma^{LS}_{\alpha\beta\mu\nu}\,I(x,y)\Sigma_{\mu\nu} + \sigma^{LE}_{\alpha\beta\mu\nu}\,I(x,y)\,E_\mu\,E_\nu. \quad (6)$$

The term $\sigma^{LS}_{\alpha\beta\mu\nu}$ is the one used in all previous DEFT devices. However, here we are interested in the change of the conductivity to first order with light intensity and to second order with electric field, the last term in (6). It is this term that will facilitate the effective steering of the wavevector.

This electrophotoconductive effect has most recently been observed by M. Luukkala et al [7]. They observed a substantial change of the photoconductivity of a CdSe film deposited on a $LiNbO_3$ substrate when a SAW was propagated on its surface. They observed the effect with 70 Mhz SAW's. There is substantial evidence that the effect is to second order in the electric field. First, they observed a change in the d.c. photoconductivity as well as observing an output at twice the SAW frequency. Second, the effect disappeared when the experiment was conducted on a non piezoelectric fused quartz substrate. This effect, also known as the Franz-Keldysh effect, has been observed in CdS by W. Franz [8] and L.V. Keldysh [9] as well as by K.S. Kohn and M.A. Lampert [10]. They also reported the effect to be quite large.

Let both the current density and the sensing d.c. electric field be in the y direction (Fig. 1). We are only interested in the σ_{yy} component of the conductivity tensor. This reduces (6) to

$$\sigma_{yy} = \sigma_L I(x,y) + \left(\sigma^{LS}_{11}\,\Sigma_2 + \sigma^{LS}_{12}\,(\Sigma_1 + \Sigma_3)\right) I(x,y) + \sigma^{LE}_{12}\,E_z\,E_z\,I(x,y) \quad (7)$$

where we used the same convention for the fourth rank conductivity tensors $\sigma^{LS}_{\alpha\beta\mu\nu}$ and $\sigma^{LE}_{\alpha\beta\mu\nu}$ as is used for the elastic constants of isotropic materials. There is both an electric field component along the propagation direction (E_x or E_y) of the SAW's and one normal to the surface of the substrate (E_z).

The interdigital contacts (indium) effectively combine all of these rectangles in parallel. Thus the current response to a constant voltage applied across the contacts results in a difference frequency term

$$i_d \propto \sum_{\substack{\text{over all}\\ \text{fingers in}\\ \text{contact}}} \sum_{\substack{\text{along}\\ \text{each long}\\ \text{rectangle}}} \sigma^{LE}_{12}\,E_z^2\,I(x,y) \quad . \quad (8)$$

As the contact fingers become numerous and very thin, we obtain the result in (1).

Thus by controlling the frequencies of the two transducers, arbitrary Fourier components can be found. The order in which the scan of Fourier space is performed is determined by the particular application.

Experimental Results

The CdS films were made in the conventional way by evaporating CdS out of a fused quartz crucible onto soda-lime glass substrates heated to 212°C. The films were then cured at 650°C under a flow of N_2, with

traces of O_2 and HCl. However, unlike the conventional method, the CdS films were Cu doped during the evaporation itself by introducing in the vacuum system a tungston boat with 50 mg of Cu heated to about 1025°C. It was found that the doping concentration could be better controlled this way than by introducing Cu during curing.

Films cured in this way were fairly reproducible and had a light to dark current ratio of about 200 at an illumination of 50 ft. cds.

The film conductivity g_0 was examined as a function of light intensity. It was found that, while the relationship was not linear, it could be fitted to a power law i.e.,

$$g = \text{const} \times I^{\alpha}. \tag{9}$$

Clearly for use in the DEFT device one would want α to be exactly one. However, the best values obtained to date for α were 0.75, which compare quite well with the values obtained for commercial CdS.

Measurements were made on the films to test the Franz-Keldysh, or electrophotoconductive effect with white light. This effect predicts that the conductivity at any given light intensity of the film should be a quadratic function of the electric field, i.e.,

$$g = g_0\left(1 + \frac{b}{g_0} E^2\right). \tag{10}$$

I-V measurements on the films showed the characteristics were in fact non-linear. Moreover, they could easily be fitted to the above expression for g and yielded the results of Table 1.

Light Intensity (Foot Candles)	b $\text{Mhos-m}^2/\square\text{-Volt}^2$	b/g_0 m^2/Volt^2
1	1.4×10^{-17}	2.5×10^{-12}
5	6.4×10^{-17}	4.0×10^{-12}
10	11.9×10^{-17}	5×10^{-12}

Table 1. Dependence of nonlinearity on light.

In the design of the Franz-Keldysh device the transducer lines have a separation of 6 microns and the oscillator peak to peak voltage is about 1 volt, corresponding to an electric field, E, of about 1.67×10^5 v/m. Thus we expect from (10) that there should be a 10% change in the conductivity of the film for the given strain at 10 foot candles, sufficient to produce a detectable signal. The actual electric fields produced by strain in the $LiNbO_3$ will be somewhat less since the conversion of applied field to the forward generated field in the SAW is not without loss.

The prototype has been built and mounted and we hope to verify the pseudo beam steering aspects in the near future.

A Pseudo Beam Steering Elastobirefringent Light Valve

Our previous work with the elastobirefringent light valve using standing acoustic waves [1,4,11], and the possibility of using pseudo beam steering to obtain arbitrary Fourier components, led to the consideration of a travelling wave elastobirefringent light valve. Fig. (2) shows a schematic view of the configuration used with the light valve to obtain the two-dimensional transform of an image.

Two orthogonal transducers are shown; one in the positive x-direction and one in the negative y-direction. The strain in the region of the lithium niobate substrate where both SAW's propagate is the linear superposition of the two travelling strain waves. Therefore, it can be expressed as

$$\Sigma = \Sigma_{x1} \cos(k_1 x - \omega_1 t) + \Sigma_{x2} \sin(k_1 x - \omega_1 t) + \Sigma_{y1} \cos(k_2 y + \omega_2 t) + \Sigma_{y2} \sin(k_2 y + \omega_2 t). \tag{11}$$

Both cosine and sine terms appear due to the compression and shear portions of the wave being ninety degrees out of phase.

An image is focused on the region of the lithium niobate where the two waves are superimposed. It is assumed that we are working in the Raman-Nath region so that the light rays remain parallel inside the material. The polarizer and analyzer are crossed to pass a minimum amount of light when no electrical signal is applied to the transducers. Since y-cut lithium niobate is used in the prototype device, the natural birefringence keeps the light from being zeroed by the crossed polarizers.

Due to the natural birefringence and the strain-induced birefringence, each ray of light splits into two orthogonally polarized rays which travel inside the material with different phase velocities. Let the phase difference between the two rays after they exit the material be δ. Then the intensity of the light I_0 at the detector in Fig. (2) is given by

$$I_0(x,y) = I(x,y) \sin^2 \frac{\delta}{2} \tag{12}$$

where I is the light intensity of the image on the lithium niobate.

The relationship of this phase difference to the strain is

$$\delta_s = \frac{\pi L p n^3}{\lambda} \Sigma \tag{13}$$

where p is a constant depending on the elasto-optical constants of the material, L is the depth of the SAW (approximately two acoustic wavelengths), n is the refractive index of the material, and λ is the wavelength of light.

We will neglect here the electrooptic effect for simplicity. A full tensor treatment of both the photoelastic and electrooptic effects does not reveal any significant differences when both are included [12]. Thus (12) can be expanded yielding

$$I_0(x,y) = I(x,y)\left[\left(\frac{\delta}{2}\right)^2 - \frac{1}{3}\left(\frac{\delta}{2}\right)^4 + \ldots\right]. \tag{14}$$

Keeping only the first term yields

$$I_0(x,y) = \frac{I(x,y)}{4} \delta^2. \tag{15}$$

The contribution of higher order terms which normally would have to be considered is not important in this case since no term except the first contributes to the difference frequency which will be detected. Neglecting the natural birefringence and substituting the phase difference from (13) and the strain, (11), yields

$$I_0(x,y) = \frac{I(x,y)}{4}\left(\frac{\pi L p n^3}{\lambda}\right)^2 [\Sigma_{x1} \cos(k_1 x - \omega_1 t) + \Sigma_{x2} \sin(k_1 x - \omega_1 t) + \Sigma_{y1} \cos(k_2 y + \omega_2 t) + \Sigma_{y2} \sin(k_2 y + \omega_2 t)]^2. \tag{16}$$

The squaring produces a term at the difference frequency which at the output of the photodetector is given by

$$i(t) = \frac{R}{4}\left(\frac{\pi L p n^3}{\lambda}\right)^2 \left\{ \iint I(x,y)[\Sigma_{x1}\Sigma_{y1} \cos(k_1 x + k_2 y) + \Sigma_{x1}\Sigma_{y2} \sin(k_1 x + k_2 y)]\, dx dy \cos[(\omega_1 - \omega_2)t] \right\} + \frac{R}{4}\left(\frac{\pi L p n^3}{\lambda}\right)^2 \left\{ \iint I(x,y)[\Sigma_{x1}\Sigma_{y1} \sin(k_1 x + k_2 y) - \Sigma_{x1}\Sigma_{y2} \cos(k_1 x + k_2 y)]\, dx dy \sin[(\omega_1 - \omega_2)t] \right\} \tag{17}$$

where R is the response of the photodetector. The magnitude of the detector current at the difference frequency is then

$$|i(t)| = \frac{R}{4}\left(\frac{\pi L p n^3}{\lambda}\right)^2 (\Sigma_{x1}^2 \Sigma_{y1}^2 + \Sigma_{x2}^2 \Sigma_{y2}^2)^{1/2} \left\{ \left[\iint I(x,y) \cos(k_1 x + k_2 y)\, dx dy \right]^2 + \left[\iint I(x,y) \sin(k_1 x + k_2 y)\, dx dy \right]^2 \right\}^{1/2}. \tag{18}$$

This is simply the magnitude of the Fourier transform of the image I(x,y) sampled at spatial frequency $\bar{k} = k_1\bar{x} + k_2\bar{y}$.

Consider a lithium niobate light valve with an avalanch photodiode detector, for which expected values are

$R = 200$ mA/w at .65 μm
$L = 2 \times 10^{-4}$ m
$p = .2$
$n = 2.2$
$\lambda = .65 \times 10^{-6}$ m
$\Sigma_{x1} = \Sigma_{y1} = \Sigma_{y2} = \Sigma_{x2} = 10^{-4}$

$A = 4 \times 10^{-4}$ m^2 (area of the image), and
$I(x,y) = 1 \times 10^{-3}$ watts integrated over A.

Then we obtain for the zero-order component, $|i(t)|_0 = 2.8 \times 10^{-6}$ amps.

Since the detector has a dark current of 50pA, components of the Fourier transform five orders of magnitude below the $k_1 = k_2 = 0$ component could theoretically be detected. Since all image intensities have transforms which go down as $1/k$ for large k, each order of magnitude corresponds to a decade of spatial frequency bandwidth. This demonstrates one important advantage of the light valve over the elastophotoconductive devices. By using a very low dark signal detector as a separate entity, a far greater spatial bandwidth can be obtained. This also effects several other advantages. The thin film devices suffer from rather large rise time and fall time due to carrier effects, thus limiting their temporal bandwidth. In practice, this limits them to use with images which do not change significantly in less than a few milliseconds. The only time limitations on the light valve system are caused by the detector since the valve responds instantaneously to the light.

The first experiments directed toward demonstrating the pseudo beam steering effect are in progress. The prominence of the nonlinearity has been demonstrated using standing bulk waves in fused quartz in place of surface waves. The second harmonics for some thirty driving frequencies were detected at the photocell. We expect the SAW device to prove superior.

Conclusion

Theoretical work strongly indicates that pseudo beam steering is an important nonlinear effect, of particular use in extracting arbitrary Fourier components of image intensities. In this paper, we have discussed two possible embodiments. One is a polycrystalline film deposited ona piezoelectric substrate; the other is a photoelastic light valve. Both employ an interaction between light and electronic charge which is modulated in a nonlinear manner by travelling surface acoustic waves. If two such waves travel orthogonally across the image plane, this electronic signal dependence on strain squared should provide sum and difference temporal frequency signals corresponding to specific spatial Fourier components of the image. The significantly nonlinear nature of these interactions has been demonstrated, and we expect to confirm the two-dimensional pseudo beam steering effect very shortly.

Another approach would be to actually generate an acoustic wave with controllable wave vector. Here there are two avenues of attack. The first is to excite two-dimensional resonant modes in a bounded acoustic cavity [1]. This is a linear approach, and large strains can be obtained. However, the modes become practically degenerate at high frequencies, the dispersion relation is nonlinear, and purely sinusoidally varying modes are not available.

The second avenue is parametric mixing of two surface waves to produce a third [1]. This effect is often very weak; the new wave does not obey the linear dispersion relation of its parents, and it tends to propagate with nonuniform amplitude in the mixing region [13,14].

Thus, in applications in which mixing or beam steering effects are required, pseudo beam steering appears to offer significant advantages. In DEFT sensors, successful implementation would permit these devices to be used in a wide range of processing functions, including full imaging, processing, and reconstruction of images.

Effective beam steering would also enable DEFT sensors to play an important role in pattern recognition [3,4], and optical system characterization. We have previously reported encouraging results on each of these applications as well as motion detection using sensors capable of scanning along only one axis in Fourier space [3,4,15,16].

References

1. P.G. Kornreich, S.T. Kowel, D.J. Fleming, N.T. Yang, A. Gupta, and O. Lewis, "DEFT: Direct Electronic Fourier Transforms of Optical Images", IEEE Proceedings, Vol. 62, pp. 1072-1087, August, 1974.
2. U.S. Patent #3,836,712 (9/17974).
3. S.T. Kowel, P.G. Kornreich, O. Lewis, A. Gupta, N.T. Yang, and R. Zawada, "DEFT: Progress on Direct Electronic Fourier Transforms of Two-Dimensional Images", RADC-TR-244, September 1974.
4. S.T. Kowel, P.G. Kornreich, O. Lewis, A. Gupta, and R. Zawada, "Progress on Two-Dimensional Direct Electronic Fourier Transform (DEFT) Devices", 1974 Ultrasonics Symposium Proceedings, pp. 763-767.
5. H. Gautier, G.S. Kino, and H.J. Shaw, "Acoustic Transform Techniques Applied to Optical Imaging", 1974 Ultrasonics Symposium Proceedings, pp. 99-103.
6. P. Kornreich, N.T. Yang, and S.T. Kowel, "A Direct Electronic Fourier Transform Device for Imaging", IEEE Proc. Letters, Vol. 61, pp. 1149-1150, August 1973.
7. M. Luukkala, P. Merilainen, and K. Saarinen, "Acousto-Resistive Effects in Thin Film CdSe/$LiNbO_3$ Delay Line System", 1974 Ultrasonics Symposium Proceedings, pp. 345-348.
8. W. Franz, Zeitschrift Fur Naturforschung, Vol. 13a, p. 484 (1958).
9. L.V. Keldysh, Sh. Eksperim. i Teor. Fiz. Vol. 34, p. 1138 (1958); English Translation Sov. Phys. JETP Vol. 7, p. 788 (1958).
10. E.S. Kohn and M. Lampert, Phys. Rev., Vol. B4, pp. 4479-4491, 1971.
11. A. Gupta, Ph.D. Dissertation, Syracuse University, 1975.
12. D. Cleverly, Ph.D. Dissertation, Syracuse University, 1976.
13. V.L. Newhouse, C.L. Chen, and K.L. Davis, "Possibility of Switching and Steering Surface Waves by Nonlinear Mixing in Anisotropic Media", J. Appl. Phys., Vol. 43, pp. 2603-2608, June 1972.
14. E.S. Furgason, V.L. Newhouse, "Nonlinear Acoustic Signal Processing in Multi-Mode Structures", 1973 Ultrasonics Symposium Proceedings, pp. 262-267.

15. S.T. Kowel, P.G. Kornreich, O. Lewis, and F.D. Kirschner, "Passive Detection of Motion Transverse to the Optical Viewing Axis", IEEE Trans. on Instrumentation and Measurement, Vol. IM-24, pp. 248-255, Sept. 1975

16. S.T. Kowel, P.G. Kornreich, and O. Lewis, "Focus Detection Using Direct Electronic Fourier Transform Sensors", Syracuse University Technical Report TR-75-9, to be published.

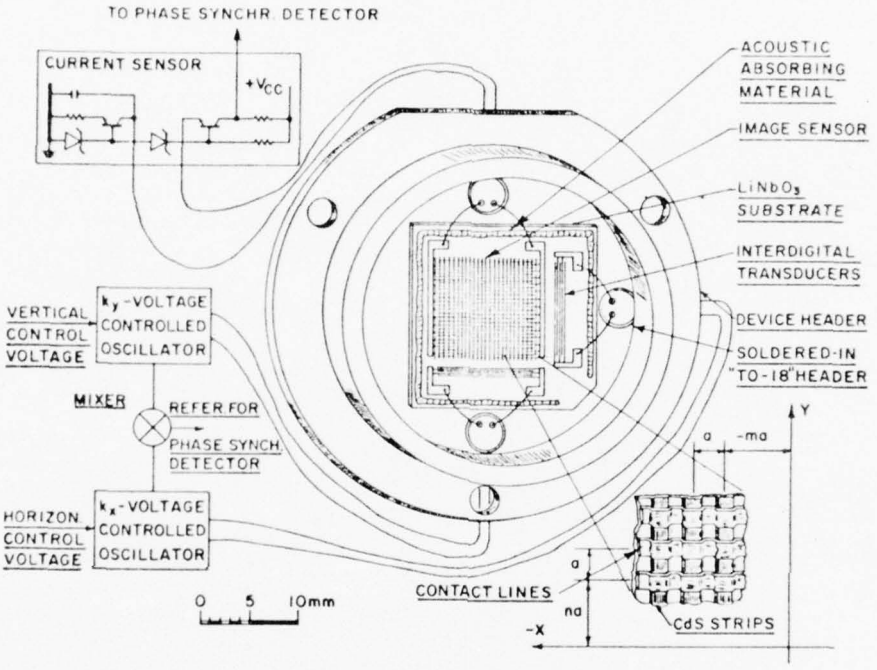

Fig. 1. Two-dimensional DEFT camera device. Note hermetically sealed construction.

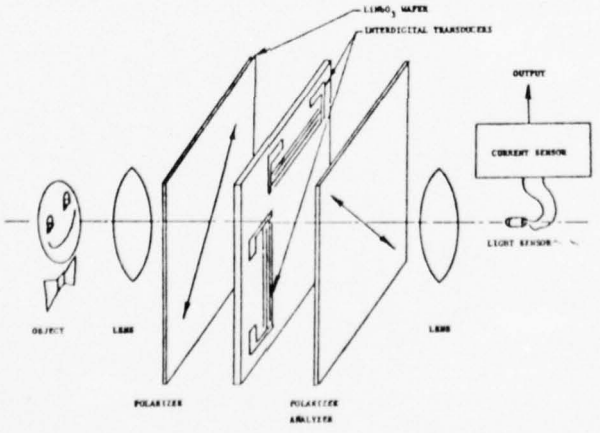

Fig. 2. Light valve sandwich DEFT imaging system. Inputs to transducers and output of current sensor make use of identical circuitry as shown in Fig. 1.

APPENDIX B

EXPERIMENTAL CONFIRMATION OF TWO DIMENSIONAL ACOUSTIC PROCESSING OF IMAGES*

S. T. Kowel, P. G. Kornreich, A. Mahapatra, and B. Emmer
Department of Electrical & Computer Engineering
Syracuse University, Syracuse, New York 13210

*1976 Ultrasonics Symposium Proceedings
IEEE Cat. #76 CHII 20 - 5SU

EXPERIMENTAL CONFIRMATION OF TWO-DIMENSIONAL ACOUSTIC PROCESSING OF IMAGES

S.T. Kowel, P.G. Kornreich, A. Mahapatra, and B. Emmer
Department of Electrical & Computer Engineering
Syracuse University, Syracuse, New York 13210

ABSTRACT. Previous acoustic processors of signals and images have been either single line or one-dimensional. Last year, we proposed a model for a two-dimensional processor using a CdS film with strong photoconductive dependence on the square of a SAW-induced electrical field. This produces coupling between two orthogonally directed SAWs yielding a current term

$$i(t) \propto \iint I(x,y)\, f_1(x-v_1t)\, f_2(y-v_2t)\, dx\, dy$$

where $I(x,y)$ is the optical intensity, and f_1, f_2 are the x and y directed surface acoustic fields respectively. The integration is provided by interdigital contacts on the film. If both SAWs are sinusoids, $i(t)$ is a spatial Fourier component of the image detected at the difference frequency.

Prototypes have been successfully fabricated and tested. Interdigital transducers with center frequencies of 27 MHz are deposited on z-cut $LiNbO_3$. The image is focused on the region in which the SAWs cross and put on a high spatial carrier frequency by a sampling grid which also serves as the electrical contact.

Qualitative tests of these devices have been made and the confirmation with theory demonstrated for sinusoidal strains yielding Fourier transforms of the image. Due to the size of these signals, this structure appears promising as a convolver as well.

Introduction

Acoustical imaging of light intensity patterns has received considerable attention; first for point-by-point scanning, and more recently for Fourier imaging.[1-4] This paper describes a novel, fully electronic, approach to the problem of extracting arbitrary, two-dimensional Fourier components of images, and reports the first experimental confirmation of this technique.

The use of surface acoustic waves to modulate photoelectrons to produce electronic signals representative of spatial Fourier components of the image offers unique advantages over other methods of Fourier imaging. Reasonable bandwidths are available and good signal-to-noise ratios can be obtained because the entire image contributes to each Fourier component. In point-by-point systems, resolution is limited by the requirement for pulse lengths of many wavelengths, and output is small due to weak electroacoustic coupling combined with small sampling area.

Careful study of all present options shows that charge coupled devices (CCD's) are likely to be far superior as spatial scanners, and optical transforming systems, although extremely powerful, are difficult to interface with electronic systems.

In order to take full advantage of SAW Fourier imaging, it is essential to be able to electronically select arbitrary, two-dimensional, Fourier components of arbitrary, two-dimensional images. Previous work has been largely confined to obtaining one-dimensional transforms of one-dimensional[2] or two-dimensional[1,3] images.[1,5] Various techniques have been proposed for achieving full two-dimensional capability, culminating in the development of the pseudo beam steering technique discussed here.

The direct electronic Fourier transform (DEFT) devices derive signals representative of Fourier components by acoustically modulating photoelectrons. In the electrophotoconductive device, two surface acoustic waves, traveling perpendicularly, cross the image, focused on a thin photoconductive film (CdS in the current model). It has been demonstrated that the absorption of light is strongly dependent on applied electric field, with the generated photocurrent having a component proportional to the square of the electric field.[6] We provide the electric fields by propagating the two crossed surface acoustic waves on a piezoelectric substrate ($LiNbO_3$) on which the CdS has been deposited. A full tensor treatment of the interaction reveals that the deposited contacts detect a current proportional to

$$i(t) \propto \iint dx\, dy\ E_z^2\,(x,y,t)\ I\,(x,y) \qquad (1)$$

where $I(x,y)$ is the image intensity, x and y are the coordinates on the film, and E_z is the electric field perpendicular to the plane.

Since

$$E_z = E_1 \cos(\omega_1 t - k_1 x) + E_2 \cos(\omega_2 t + k_2 y) \qquad (2)$$

where E_1, ω_1, k_1, refer to the x-directed acoustic wave and E_2, ω_2, k_2, refer to the y-directed acoustic wave, E_z^2 contains a term of the form

$$E_{zd}^2 \propto E_1 E_2 \cos[(\omega_1 - \omega_2)t - (k_1 x + k_2 y)]$$

$$= E_1 E_2 \cos[(\omega_1 - \omega_2)t - \bar{k}\cdot\bar{r}]. \qquad (3)$$

By varying the driving frequencies, we can vary $\bar{k}$, yielding a signal term proportional to the two-dimensional Fourier transform,

$$i_s(t) \propto \exp[j(\omega_1 - \omega_2)t] \int d^2\bar{r}\ I(\bar{r})\exp(-j\bar{k}\cdot\bar{r}) \qquad (4)$$

while the other terms from (1) can be ignored because they are at different frequencies. That is, the signal behaves as if a new acoustic wave has been created with wavevector equal to the sum of the excited wavevectors. Thus we call this effect "pseudo beam steering."

From theoretical considerations alone, pseudo beam steering is likely to be far superior to other proposed techniques for accomplishing two-dimensional imaging. For example, the actual creation of a third surface wave from nonlinear mixing appears to be a much smaller and less controllable effect.

It is clear that by using either colinear signals, or orthogonal signals, such an effect could also be the basis of a monolithic convolver.

The use of high frequency surface wave transducers requires that the image be placed on a high spatial frequency carrier. This is accomplished in one direction by the interdigital contact pattern used to detect the signal, and in the perpendicular direction by either etching the CdS into strips, or by projecting the image

1976 Ultrasonics Symposium Proceedings
IEEE Cat. #76 CHII 20 - 5SU

through a grid. Sampling with a projected grid also effects an improvement in the light-to-dark signal ratio.[2] Of course this type of sampling produces a sinc function weighting of the output. However, our devices are designed to work well within the rather broad band of that function.

Evaporation of high quality CdS films on $LiNbO_3$, curing the films, the deposition of the contact metallization, and the photolithographic lift-off had not previously been attempted on z-cut $LiNbO_3$. This material was chosen for its surface wave propagation properties.

We believe that we have solved the major problems and are now attacking the yield problem. Our results at this point are crude, but highly encouraging. We have constructed a camera system in a box the size of an 8 mm movie camera. The only external equipment needed is a power supply, a low frequency sweep generator, and a display. The signals measured are large and repeatable. Quantitative results must await further improvements.

The Electrophotoconductive Sensor

The image sensor consists of a CdS film deposited on a z-cut $LiNbO_3$ substrate as shown in Fig. (1). Thin film indium contacts, in the form of an interdigital pattern, are deposited onto the CdS film. This pattern facilitates the collection of the total photocurrent over the area of the CdS film. Indium is used as the contact material. It is our experience that indium makes ohmic contact to CdS. Aluminum pads must then be deposited over the indium before wires can be bonded.

Besides providing electrical contact, the contacts also form a grating across the image. This, in effect, shifts the Fourier transform of the image along the k_y direction to higher spatial frequencies. This allows us to generate the Fourier transform of the image with SAW's with a limited bandwidth. A similar effect is obtained along the k_x direction by etching CdS into lines along the x direction, for cured CdS. For uncured CdS, the second grid must be projected optically in order not to shift the dark current transform along with the light current signal. We use, for simplicity, gratings with equal dark and light spacings. Unfortunately, this type of grating only exposes 1/4 of the CdS film to the image. Larger film exposures are possible by making the dark areas of the masks narrower.

Since the photoconductivity of CdS has a term that depends on the square of the electric field, it is possible to obtain a mixing of the electric fields due to the two acoustic waves traveling perpendicularly to each other. This effect provides the effective steering of the wavevector, $\bar{k}$, of the transform.

Although the various electric field and strain effects may vary through the thickness of the CdS film, we shall assume all effects to be uniform. Thus, the $\alpha\beta$ component of the conductance per square can be expanded to first order in the light intensity I(x,y) and in the component of the strain tensor $\Sigma_{\mu\nu}$, and to second order in the electric field components E_μ, due to the SAW in the piezoelectric $LiNbO_3$ substrate, to yield

$$\sigma_{\alpha\beta}(x,y) = \sigma^{D}_{\alpha\beta} + \sigma^{DS}_{\alpha\beta\mu\nu}\Sigma_{\mu\nu} + \sigma^{L}_{\alpha\beta}I(x,y) + \sigma^{LS}_{\alpha\beta\mu\nu}I(x,y)\Sigma_{\mu\nu} + \sigma^{DF}_{\alpha\beta\mu}E_\mu + \sigma^{LF}_{\alpha\beta\mu}I(x,y)E_\mu + \sigma^{DE}_{\alpha\beta\mu\nu}E_\mu E_\nu + \sigma^{LE}_{\alpha\beta\mu\nu}I(x,y)E_\mu E_\nu \ldots \quad (5)$$

where summation over like Greek indices is implied. Here

$\sigma^{D}_{\alpha\beta}$ is the dark conductance per square,

$\sigma^{DS}_{\alpha\beta\mu\nu}$ is the change of the dark conductance per square with strain $\Sigma_{\mu\nu}$,

$\sigma^{L}_{\alpha\beta}$ is the change of the conductance per square with light flux I(x,y), the ordinary photoconductivity,

$\sigma^{LS}_{\alpha\beta\mu\nu}$ is the change of the conductance per square with light and strain,

$\sigma^{DF}_{\alpha\beta\mu}$ is the linear change of the conductance per square with electric field,

$\sigma^{LF}_{\alpha\beta\mu}$ is the linear change of the conductance per square with light and electric field,

$\sigma^{DE}_{\alpha\beta\mu\nu}$ is the change of the conductance per square to second order with the electric field, and

$\sigma^{LE}_{\alpha\beta\mu\nu}$ is the change of the conductance per square to first order in the light intensity and second order in the electric field.

Our polycrystalline CdS films have essentially isotrophic symmetry. Therefore all 3rd rank tensors must be zero. This requires that $\sigma^{DF}_{\alpha\beta\mu}$ and $\sigma^{LF}_{\alpha\beta\mu}$ be zero. This also requires that ordinary photoconductivity be essentially a scalar, σ_L. The dark conductance is small compared to the photoconductance at reasonable light levels for good photoconductive CdS. This allows us to neglect the terms $\sigma^{D}_{\alpha\beta}$, $\sigma^{DS}_{\alpha\beta\mu\nu}$, and $\sigma^{DE}_{\alpha\beta\mu\nu}$. This reduces (5) to

$$\sigma_{\alpha\beta}(x,y) = \sigma_L\delta_{\alpha\beta}I(x,y) + \sigma^{LS}_{\alpha\beta\mu\nu}I(x,y)\Sigma_{\mu\nu} + \sigma^{LE}_{\alpha\beta\mu\nu}I(x,y)\,E_\mu E_\nu. \quad (6)$$

The term $\sigma^{LS}_{\alpha\beta\mu}$ is the one used in all previous DEFT devices. However, here we are interested in the change of conductivity to first order with light intensity and to second order with electric field, the last term in (6). It is this term that will facilitate the effective steering of the wavevector.

This electrophotoconductive effect has been observed most recently by M. Luukkala et al[6]. They observed a substantial change of the photoconductivity of a CdSe film deposited on a $LiNbO_3$ substrate when a SAW was propagated on its surface. They observed the effect with 70 MHz SAW's. There is substantial evidence that the effect is to second order in the electric field. First, they observed a change in the d.c. photoconductivity as well as observing an output at twice the SAW frequency. Second, the effect disappeared when the experiment was conducted on a non-piezoelectric fused quartz substrate. This effect, also known as the Franz-Keldysh effect, has been observed in CdS by W. Franz[7] and L.V. Keldysh[8] as well as by K.S. Kohn and M.A. Lampert[9]. They also reported the effect to be quite large.

Let both the current density and the sensing d.c. electric field be in the y direction (Fig. 1). We are only interested in the σ_{yy} component of the conductivity tensor. This reduces (6) to

$$\sigma_{yy} = \sigma_L I(x,y) + (\sigma^{LS}_{11}\Sigma_2 + \sigma^{LS}_{12}(\Sigma_1 + \Sigma_3))I(x,y) + \sigma^{LE}_{12}E_zE_zI(x,y) \quad (7)$$

where we used the same convention for the fourth rank conductivity tensors $\sigma^{LS}_{\alpha\beta\mu\nu}$ and $\sigma^{LE}_{\alpha\beta\mu\nu}$ as is used for the elastic constants of isotropic materials. There is both an electric field component along the propagation direction (E_x or E_y) of the SAW's and one normal to the surface of the substrate (E_z). Only the E_z^2 term is included since, of all the possible products of electric fields, it is the only one at the difference frequency which contributes to σ_{yy}.

The interdigital contacts (indium) effectively combine all of these rectangles in parallel. Thus the current response to a constant voltage applied across the contacts results in a difference frequency term

$$i_d \propto \sum_{\substack{\text{over all}\\ \text{fingers in}\\ \text{contact}}} \sum_{\substack{\text{along}\\ \text{each long}\\ \text{rectangle}}} \sigma_{12}^{LE} E_z^2 I(x,y). \qquad (8)$$

As the contact fingers become numerous and very thin, we obtain the result in (1).

Thus, by controlling the frequencies of the two transducers, arbitrary Fourier components can be found. The order in which the scan of Fourier space is performed is determined by the particular application.

Experimental Results

The majority of our efforts were directed to evaporating and curing CdS films. The curing vastly improves the light-to-dark conductivity ratio.

It soon became clear that the technique used on $LiNbO_3$ could not be the same as that used on glass. The film characteristics depend strongly on the substrates used. During curing material diffuses out of the substrate into the film. For example, sodium diffuses out of glass. The characteristics of the films change considerably depending on whether these diffused materials form trapping centers, recombination centers, or sensitizing centers.

On the glass substrates[1] CdS was evaporated out of a fused quartz bottle onto suitably positioned substrates in a vacuum of 10^{-5} torr. These evaporated films had very high conductivities but a very poor light-to-dark ratio. To increase their sensitivity they were cured at 650°C under a N_2 flow which had traces of O_2 and HCl in it. At the same time the film was Cu doped by placing it in a quartz boat which had about 25 grams of CdS plus 12.5 grams of Cu in it. Many experiments were conducted by altering the amounts of HCl, O_2 and Cu, to optimize the photoconductivity properties of the films. We finally succeeded in obtaining ratios of about 1000 at 25 ft. candles. At the same time, the conductivity of the films was quite high -- about 1 nanomho/□ . This is essential to obtain reasonable signals with sensor contact lines having about 20,000 squares.

We hoped that by suitably adjusting the doping levels of O_2, HCl and Cu, one could get good photoconducting films of CdS on $LiNbO_3$. However, after numerous attempts, we came to the conclusion that this is not possible since it is difficult to overcome the degrading effect of material diffusing out of the $LiNbO_3$ during curing.

Next we decided to overcome the problem of the substrate entirely, by laying down a thin layer of SiO_x between the substrate and the CdS film. This layer would insulate the CdS from the $LiNbO_3$. At the same time, SiO_x, being very stable thermally, would not diffuse into the CdS. This idea proved very successful since we improved the light-to-dark ratio of our films by a factor of 100 in the first few attempts. We are still working on optimizing various doping levels.

Unfortunately, the SiO_x layer had its own problems. It works well with y-cut $LiNbO_3$, which has a low thermal coefficient of expansion like the SiO but on z-cut $LiNbO_3$, which has a coefficient of expansion about 10 times that of y-cut, the films tend to peel off during curing. However, one would prefer to use the z-cut $LiNbO_3$ since it has better acoustic properties. Only z-cut offers two equally viable surface wave propagation directions with equal velocities.

At this point, a number of attempts to prevent the CdS from peeling off of the SiO_x have been unsuccessful. These include graduating the SiO_x-CdS boundary during evaporation, and roughening the surface of the $LiNbO_3$. We are currently trying two new approaches to the problem of CdS peeling during curing. One is out-diffusing the $LiNbO_3$ substrate before evaporation. This would obviate the need for the SiO_x film. The other approach is to use a film of Alumina under the CdS. Alumina is used commercially as a substrate for cured CdS in photodetectors.

Because of the problem of keeping CdS on $LiNbO_3$ after curing, we have also tried an alternate approach. We deposited CdS films on z-cut $LiNbO_3$, and dispensed with curing. The CdS was not etched into lines, but the contacts and transducers were fabricated in the usual manner. Uncured CdS has a poor light-to-dark conductivity ratio since it has not been recrystallized. However, by putting the dark current on a different spatial carrier frequency than the light-induced current, a substantial improvement in light-to-dark signal can be obtained. This is accomplished by projecting the optical image through a mask which samples in the direction perpendicular to the contact fingers. Thus the dark current is translated along one axis in k-space, while the light current is translated off this axis into a different region of k-space.

The first device of this type had a light-to-dark conduction ratio of 0.01. Thus the improvement afforded by sampling was not sufficient to obtain significant light sensitivity. However, the response to dark current was very large, establishing that the uncured films exhibit a large Franz-Keldysh effect. Indeed, one found that in these films $\sigma_{DE}/\sigma_D = 0.47$.

Fig. (2) shows a typical scan of frequency space for this device. With no drive to the transducers, we obtained plain circles. With the transducers excited, these circles exhibit strong vertical modulation. This display is obtained by sinusoidally exciting each transducer with a voltage controlled oscillator. These two oscillators are in turn driven by a slowly varying (300 Hz) external sinusoidal generator, with a phase difference of 90° introduced between them. This produces the circular scans of k-space seen in the figure. The particular circle radius is controlled by the amplitude of the sweep generator. The output of the device is shown as the vertical height above, or below, the circle. Each point on the circle represents a specific temporal frequency difference and a specific spatial frequency.

The second device was fabricated identically, except that additional sulphur was introduced during evaporation. This produced a film with light-to-dark conductivity ratio of approximately 10. This device suffered film peeling, probably caused by insufficient substrate preparation and/or by an unusually high level of air pollution in the laboratory. Thus only a small portion, approximately 5% of the film remained usable. The Franz-Keldysh coefficient, however, was as large as in the previous device, and it was mounted in the camera and tested. Fig. (3) shows typical results of frequency scans with this device. Note the difference between the scans with and without light. By changing the external sweep function; arbitrary scans can be designed, making the device random access. One reason for the odd symmetries exhibited is that the voltage versus frequency curve for our voltage controlled oscillator is nonlinear, as shown in Fig. (4).

These results, though qualitative and rather crude, are highly satisfying. The signals are large, even in the uncured films; are detected at the difference frequencies of the two transducers; and are image dependent.

We measured the following characteristics for the devices described:

Surface wave speed	3635 m/s
Center frequency	28.62 MHz
CdS sensor size	12.7 mm x 12.7 mm
Sensor plus transducers	17 mm x 17 mm

contact grid periodicity 0.127 mm.

The transducers were fifteen finger-pair, apodized indium contacts.

Conclusions

We have shown experimentally that a strong signal of the form of the integral of the product of an electron distribution multiplied by the product of two surface acoustic wave fields can be obtained on CdS films,

$$i(t) \propto \iint I(x,y) f_1(x - v_1 t) f_2(y - v_2 t) dx dy.$$

Clearly this effect can be used for imaging by choosing the acoustic fields, f_1, f_2, to be scanning pulses, and for Fourier imaging if f_1, f_2 are sinusoids. Such a device could also be used as a monolithic convolver. We have shown this effect to be large even in uncured sulphur-rich films of CdS. Light sensitivity could play a role in the convolver application by providing frequency manipulation.

We are continuing to try to improve the yield by improving the adhesion of the films. With this accomplished, the crude prototypes described here could be improved sufficiently to enable devices of this type to be used in a wide range of applications.

Acknowledgement

The authors wish to acknowledge the support of the National Science Foundation and of the U.S. Army Night Vision Laboratory, Ft. Belvoir, VA. We are also grateful for the interest and encouragement of the U.S. Army Topographic Engineering Laboratory, Ft. Belvoir.

Thanks are due to Thomas Martel, John Wood, and Paul Reck for their assistance in carrying out the measurements described in this paper.

References

1. P.G. Kornreich, S.T. Kowel, D.J. Fleming, N.T. Yang, A. Gupta and O. Lewis, "DEFT: Direct Electronic Fourier Transforms of Optical Images," IEEE Proceedings, Vol. 62, pp. 1072-1087, August, 1974.
2. H. Gautier, G.S. Kino and H.J. Shaw, "Acoustic Transform Techniques Applied to Optical Imaging," 1974 Ultrasonics Symposium Proceedings, pp. 99-103.
3. S.T. Kowel, P.G. Kornreich, A. Mahapatra, D. Cleverly B. Emmer, and R. Zawada, "Two-Dimensional Fourier Imaging of Light Using Acoustic Pseudo Beam Steering," 1975 Ultrasonic Symposium Proceedings, pp. 136-140.
4. J.K. Elliott, R.L. Gunshor, R.F. Pierret and K.L. Davis, "Characteristics of Zinc Oxide-Silicon Surface Wave Convolvers for Optical Imaging and Memory," 1975 Ultrasonic Symposium Proceedings, pp. 141-143.
5. S.T. Kowel, P.G. Kornreich, O. Lewis and F.D. Kirschner, "Passive Detection of Motion Transverse to the Optical Viewing Axis," IEEE Trans. on Instr. and Meas., Vol. IM-24, No. 3, pp. 248-255, Sept.'75
6. M. Luukkala, P. Merilainen and K. Saarinen, "Acousto-Resistive Effects in Thin Film CdSe/$LiNbO_3$ Delay Line System," 1974 Ultrasonic Symposium Proceedings, pp. 345-348.
7. W. Franz, Zeitschrift Fur Naturforschung, Vol. 13a p. 484 (1958).
8. L.V. Keldysh, Sh. Exsperim i Teor. Fiz. Vol. 34, p. 1138 (1958); English Translation Sov. Phys.JETP Vol. 7, p. 788 (1958)
9. E.S. Kohn and M. Lampert, Phys. Rev., Vol. B4, pp. 4479-4491, 1971.

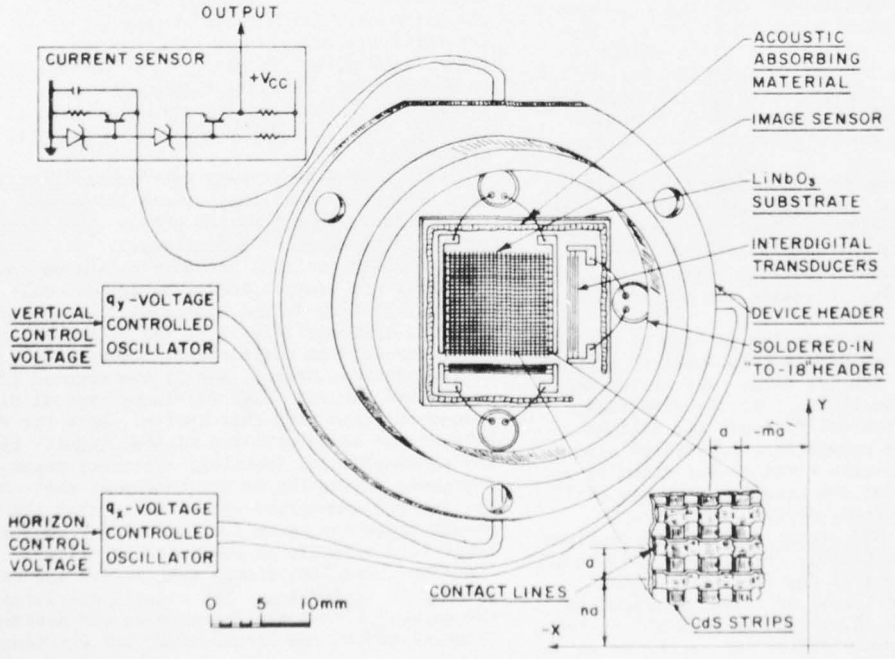

Fig. (1). Schematic of two-dimensional DEFT sensor. The data shown in Fig. (3) were taken using a device for which the CdS was not etched into strips.

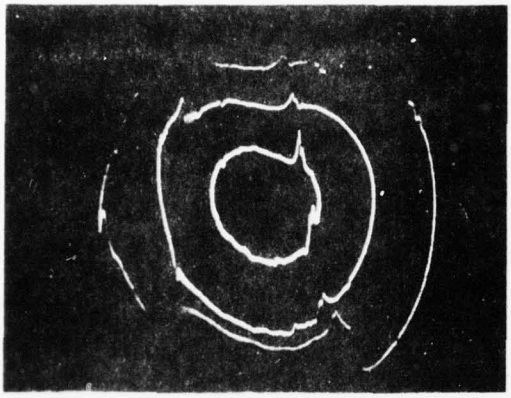

Fig. (2). Spatial frequency scan of dark current. Vertical modulation of circles is due to transform of a circular imperfection in the CdS film.

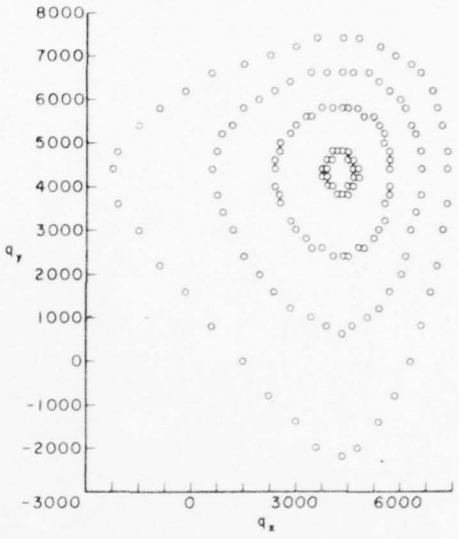

Fig. (4). Actual spatial frequencies in inverse meters of typical curves represented by circles in Fig. (2) and Fig. (3). Note the asymmetries caused by the nonlinear behavior of the voltage controlled oscillators, and the lack of proper alignment of the sweep center with the center of the image Fourier space, $q_x = q_y = 0$. These q variables are defined by $q_x = k_x - (2\pi/a)$, and $q_y = k_y - (2\pi/a)$, where a is the period of the sampling.

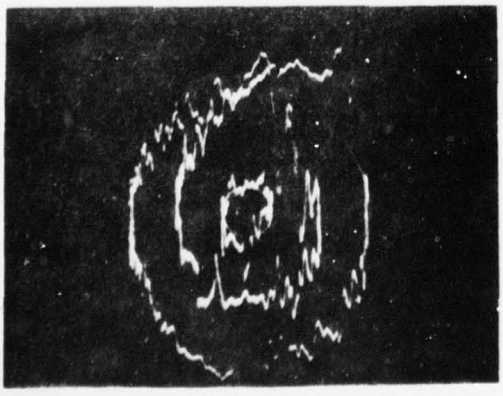

Fig. (3a)

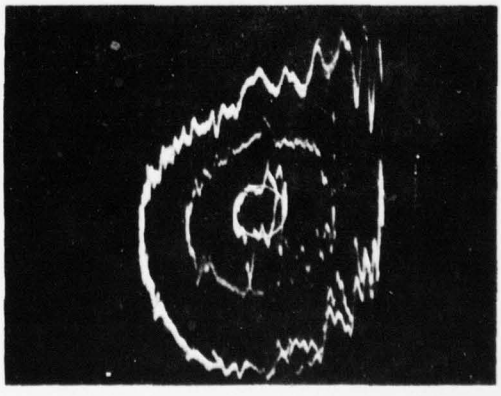

Fig. (3b)

Fig. (3). Response of light-sensitive device. Both light and dark currents are sampled only by the contact fingers, so no enhancement occurs. The complex patterns are caused by the severe nonuniformities of the CdS film. Fig. (3a) is for the device in the dark, while Fig. (3b) is for the illuminated device. Note that traces represent amplitudes, rather than magnitudes, of the Fourier components.

APPENDIX C

PHENOMENOLOGICAL CALCULATION OF THE CONDUCTANCE OF CdS

Though we realize that various electric field and strain effects may vary through the thickness of the CdS film, we shall, for simplicity, assume all effects to be uniform over the thickness of the CdS film. Thus, the conductance per square can be expanded in a Taylor series to first order in the light intensity $I(x, y)$ and the strain tensor $\Sigma_{\mu\nu}$ and to second order in the electric field E_μ, due to the SAW in the piezoelectric $LiNbO_3$ substrate.

$$\begin{aligned}\sigma_{\alpha\beta}(x, y) = {} & \sigma^{D}_{\alpha\beta} + \alpha^{DS}_{\alpha\beta\mu\nu}\,\Sigma_{\mu\nu} + \sigma^{L}_{\alpha\beta}\,I(x, y) + \sigma^{LS}_{\alpha\beta} + I(x, y)\Sigma_{\mu\nu} \\ & + \sigma^{DF}_{\alpha\beta\mu}\,E_\mu + \sigma^{LF}_{\alpha\beta\mu}\,I(x, y)E_\mu + \sigma^{DE}_{\alpha\beta\mu\nu}\,E_\mu\,E_\nu \qquad \text{(C.1)} \\ & + \sigma^{LF}_{\alpha\beta\mu\nu}\,I(x, y)E_\mu\,E_\nu \ldots\end{aligned}$$

where summation over like Greek indices is implied.

Here

- $\sigma^{D}_{\alpha\beta}$ is the dark conductance per square,
- $\sigma^{DS}_{\alpha\beta\mu\nu}$ is the change of the dark conductance per square with strain $\Sigma_{\mu\nu}$,
- $\sigma^{L}_{\alpha\beta}$ is the change of the conductance per square with light flux $I(x, y)$, the ordinary photoconductivity.
- $\sigma^{LS}_{\alpha\beta\mu\nu}$ is the change of the conductance per square with light and strain,
- $\sigma^{DF}_{\alpha\beta\mu}$ is the linear change of the conductance per square with electric field,
- $\sigma^{LF}_{\alpha\beta\mu}$ is the linear change of the conductance per square with light and electric field,
- $\sigma^{DE}_{\alpha\beta\mu\nu}$ is the change of the conductance per square to second order with electric field, and

$\sigma^{LE}_{\alpha\beta\mu\nu}$ is the change of the conductance per square to first order in the light intensity and second order in the electric field.

Our polycrystalline CdS films have essentially isotropic symmetry. Therefore all 3rd rank tensors must be zero.[16] This requires that $\sigma^{DF}_{\alpha\beta\mu}$ and $\sigma^{LF}_{\alpha\beta\mu}$ be zero. This also requires that the ordinary photoconductivity be essentially a scalar, $\sigma_L \delta_{\alpha\beta}$. The dark conductance is small compared to the photoconductivity at reasonable light levels for good photoconductive CdS. This allows us to neglect the terms $\sigma^{D}_{\alpha\beta}$, $\sigma^{DS}_{\alpha\beta\mu\nu}$, and $\sigma^{DE}_{\alpha\beta\mu\nu}$. This reduces (C.1) to

$$\sigma_{\alpha\beta} = \sigma_L \delta_{\alpha\beta} I(x, y) + \sigma^{LS}_{\alpha\beta\mu\nu} I(x, y) \Sigma_{\mu\nu} + \\ + \sigma^{LE}_{\alpha\beta\mu\nu} I(x, y) E_\mu E_\nu . \qquad \text{(C.2)}$$

The term $\sigma^{LS}_{\alpha\beta\mu\nu}$ is the one that has been used in all our previous DEFT devices. However, here we are interested in the change of the conductivity to first order with light intensity and to second order with electric field, the last term in (C.2). It is this term that will permit the effective steering of the wave vector, $\vec{k}$.

A similar effect has previously been observed by M. Luukkala et.al[11]. They observed a substantial change of the photoconductivity of a CdSe film deposited on a $LiNbO_3$ substrate when a SAW was propagated on its surface. They observed the effect with 70 MHz SAWs. There is substantial evidence that the effect is to second order in the electric field. They observed a change in the d.c. photoconductivity as well as observing an output at twice the SAW frequency; and the effect disappeared when the experiment was conducted on a non-piezoelectric fused quartz substrate. The effect also known as the Franz-Keldysh effect has been observed in CdS by W.

Franz[13] and L. V. Keldysh[14] as well as by E. S. Kohn and M. A. Lampert[15]. They also reported the effect to be quite large.

The electric field E_μ due to the surface acoustic wave in the piezoelectric substrate has the form

$$E_1 = E_{Ax} = E_{1x} \cos(\omega_1 t - k_1 x).$$

$$E_2 = E_{Ay} = E_{2y} \cos(\omega_2 t + k_2 y). \qquad (C.3)$$

$$E_3 = E_{Az} = E_{1z} \cos(\omega_1 t - k_1 x) + E_{2z} \cos(\omega_2 t + k_2 y)$$

Note that the y directed wave is propagating in the negative y direction. The applied d.c. electric field E_0 applied at the pickup contact is in the y direction. The component of the surface current density K_μ in the CdS film is given by *Ohm's Law*

$$K_\mu = \sigma_{\mu\nu} E_\nu \qquad (C.4)$$

where $\sigma_{\mu\nu}$ is given by (C.2). However, we detect the y component of the current density,

$$K_y = \sigma_{xy} E_{Ax} + \sigma_{yy}(E_0 + E_{Ay}) + \sigma_{yZ} E_{Az}. \qquad (C.5)$$

Assuming that the CdS film has isotropic symmetry in the plane of the film, the xy plane, but has a unique axis normal to the film in the z direction, the photoconductivity tensor components of interest and using the matrix notation of elasticity[16],

$$\sigma_{xy} = I(x, y)\sigma_{44}^{LE} E_{Ax}(E_{Ay} + E_0) \qquad (C.6)$$

$$\sigma_{yy} = I(x, y)\sigma_L + I(x, y)\sigma_{12}^{LE} E_{Ax}^2 + I(x,y)\sigma_{11}^{LE}(E_{Ay} + E_0)^2$$

$$+ I(x, y)\, \sigma_{13}^{LE} E_{Az}^2 \qquad (C.7)$$

$$\sigma_{yz} = I(x, y)\ \sigma_{66}^{LE}\ (E_{Ay} + E_0)E_{Az} \tag{C.8}$$

where, for the moment, we neglect the small strain dependent photoconductivity terms $\sigma_{\alpha\beta\mu\nu}^{LS}$. Substituting (C.6), (C.7), and (C.8) into (C.5) we obtain for the surface current density

$$\begin{aligned} K_y = I(x, y)\{&\sigma_L E_0 + \sigma_{11}^{LE}\ E_0^3 + \sigma_L E_{Ay} + 3\sigma_{11}^{LE}\ E_0^2\ E_{Ay} + \\ &+ [(\sigma_{44}^{LE} + \sigma_{12}^{LE})E_{Ax}^2 + 3\sigma_{11}^{LE}\ E_{Ay}^2 + (\sigma_{13}^{LE} + \sigma_{66}^{LE})E_{Az}^2]E_0 \\ &+ \sigma_{44}^{LE}\ E_{Ax}^2\ E_{Ay} + \sigma_{11}^{LE}\ E_{Ay}^3 + [\sigma_{13}^{LE} + \sigma_{66}^{LE}]E_{Az}^2\ E_{Ay}\}. \end{aligned} \tag{C.9}$$

From (C.3) and (C.9) one can observe current components oscillating with the following frequencies

$$\begin{gathered} \text{zero} \\ \omega_1 - \omega_2 \\ \omega_1 \\ \omega_2 \\ 2\omega_1 - \omega_2 \\ 2\omega_2 - \omega_1 \\ 2\omega_1 \\ 2\omega_2 \\ 2\omega_1 + \omega_2 \\ 2\omega_2 + \omega_1 \\ 3\omega_2 \\ \omega_1 + \omega_2 \end{gathered}$$

The d.c. component of the surface current density is

$$\begin{aligned} K_{y0} = [&\sigma_L + \sigma_{11}^{LE}\ E_0^2 + \tfrac{1}{2}\ (\sigma_{44}^{LE} + \sigma_{12}^{LE})E_{1x}^2 + \tfrac{3}{2}\sigma_{11}^{LE}\ E_{1y}^2 \\ &+ \tfrac{1}{2}\ (\sigma_{13}^{LE} + \sigma_{66}^{LE})(E_{1z}^2 + E_{2z}^2)]I(x, y)E_0. \end{aligned} \tag{C.10}$$

There is only one term oscillating with the difference frequency, $\omega_1 - \omega_2$,

$$K_{sig} = I(x, y)(\sigma_{13}^{LE} + \sigma_{66}^{LE})E_{1z} E_{2z} E_0 \cos[(\omega_1 - \omega_2)t - (k_1 x + k_2)]. \quad (C.11)$$

However, note the fact that for $\omega_1 > \omega_2$, that is $k_1 > k_2$, the above conductivity wave propagates in the positive k_α direction. For $\omega_2 > \omega_1$, that is $k_2 > k_1$, the wave propagates in the negative k_α direction.

CdS FILM FABRICATION

D.1. Fabrication on Glass

Here we give the recipe for making films, including curing and cleaning stages. To some extent, the steps are specific to our set-up and equipment. However, because of the significance of the development of the layered technique, we decided to give the recipe intact. Others knowledgeable in this field should be able to implement equivalent steps in their laboratories.

A) Cleaning of substrates:

(1) Clean substrates with soap, then with "micro".

(2) Rinse in superQ H_2O at least 15 minutes.

(3) Put in ultrasonic cleaner with acetone 15 minutes.

(4) Rinse in superQ H_2O 15 minutes.

(5) Blow dry with filtered N_2.

B) Evaporation of CdS

(1) Fill one of the quartz bottles with about 3 grms. CdS using dropper.

(2) Mount bottle with "wrap-around" molybdenum filament in electrodes 2 and 5 of vacuum system.

(3) Surround bottle with fused quartz chimney.

(4) Cover chimney with stainless-steel lid so that neck of bottle just fits hole in the center.

(5) Mount substrates in the holder.

(6) Assemble base-plate, chimney and substrate holder in vacuum system.

(7) Insert thermocouple into substrate holder and connect heaters to electrodes 3 and 4 of substrate holder for maintenance of substrate temperature.

(8) Close vacuum system and flush thrice with N_2.

(9) Adjust substrate heater assembly as explained below and heat substrates to about 212°C.

(10) Gradually (10 minutes) bring power in evaporation filament to 370W.

(11) Open shutter, evaporate for one hour.

(12) Close shutter and switch off all power supplies.

(13) Let substrates cool to room temperature before removing from vacuum system. Leave them in the vacuum system overnight.

Note: We have not used the tungsten boat or the new thickness monitoring system to evaporate CdS on glass. This, of course, would be the logical thing to do. To do this, after step (7) above go through steps in D.2 point B for evaporation of CdS on $LiNbO_3$.

C) Curing of films: (For a three inch diameter diffusion furnaces)

(1) The furnance heater settings should be as follows:

Left	Center	Right
580	178	580

These settings, presumably, result in a temperature of 647°C $\pm$ 8°C over a sufficiently large region of the furnance tube. FURNACE IS ALWAYS KEPT ON!!

(2) Set gas flow-rates as follows:

N_2 = 12 cms. (steel ball) (few litres/min.)

O_2 = 3.5 cms. (black ball)

HCL = 4.5 cms. (steel ball)

This process can be tricky since balls tend to move up and down for about 30 minutes before finally settling down to steady values. So check on them every five minutes. To start 0_2 flow, open four valves - one on the 0_2 cylinder, two lever-type valves on the dryer next to the cylinder, one on the flow meter. The N_2 cylinder valve is always open, so you open only the flow meter valve. HCl - open only the flow meter valve.

(3) Two boats are used in the curing process. The first one has 25 gms. of CdS and 12.5 gms. of Cu in each of two small boats placed on the CdS. Push this boat into the furnace with its nearer end 26" from the end of the furnace tube.

(4) Place the glass substrate on a fused quartz substrate (with a thin layer of quartz wool in between); then place both in the 2nd boat. Follow the time-table given below:

(a) 0 mins. - CdS and Cu boat in place

(b) 10 mins. - start pushing boat holding substrate into furnace

(c) 15 mins. - substrate should be in place . Close mouth of furnace with pyrex wool ball.

(d) 45 mins. - shut off 0_2 and HCl and set N_2 to 9 cms. [Close all four 0_2 valves!!!]

(e) 105 mins. - start pulling out substrate boat

(f) 115 mins. - substrate boat out of furnace. Place in N_2 chamber and flush 2 mins. with N_2. Hold on to the "stopper" or "cap" when you do this. The N_2 pressure may blow it off!!!

(g) Let substrate cool in N_2 chamber for 30 mins. Take it out. Pull out CdS and Cu boat - cool at mouth of furnace for 5 mins. Place in N_2 chamber, flush for 2 mins. Turn down N_2 to 2 cms. (black ball). This is the usual setting when furnace is not in use.

D) Additional Tips on Curing of CdS:

(1) If the films cured come out black and have high light and dark conductivities (L/D small) they probably have too much Cl_2. Reduce HCl setting. Changing HCl setting from 4.5 cm. to 4.0 cm. is a "big" change.

(2) If the cured films look yellowish, have good L/D ratios but light conductivity is low, there is probably too little Cl_2. Increase HCl setting.

D.2. Two Layer Film Fabrication on $LiNbO_3$

A) Cleaning of Substrates

(1) use same process as for glass

(2) Use a more elaborate technique if you deem it necessary.

B) Evaporation of CdS

(1) Fill the two compartments in the tungsten boat with about 3 gms. of CdS.

(2) Mount boat in electrodes 2 and 5 of vacuum system.

(3) Surround boat with fused quartz chimney.

(4) Mount $LiNbO_3$ substrates in holder using the aluminium holders available.

(5) Assemble base-plate, chimney and substrate holder in vacuum system.

(6) Insert thermocouple and connect heaters to electrodes 3 and 4.

(7) Make sure the thickness monitoring head is "looking" at the evaporation boat and that it is receiving cooling water.

(8) Close vacuum system and flush thrice with N_2.

(9) Adjust substrate heater assembly and heat substrates to about 212°C.

(10) Turn on power to thickness moniter. Deposition rate should read 000 A°/sec and thickness should read 0000 or 9999 A°.

(11) Gradually bring power in evaporation boat to 370 W.

(12) Open shutter and adjust filament power to get a steady deposition rate of about 14 A°/sec.

(13) Evaporate to a thickness of 4.5μ = 45000 A°. (Uncalibrated).

(14) Close shutter, switch off power supplies.

(15) Let substrates sit in vacuum system overnight before removing.

D. 3 Curing of Films

Follow steps C1 through C4 given for curing of films on glass except for the following changes:

(a) Set gas flow rates as follows:

N_2 = 12 cms. (steel ball)

O_3 = 1.7 cms. (black ball)

HCl = 1.3 cms. (steel ball)

(b) Hold $LiNbO_3$ substrates in a vertical position using one of the grooved fused quartz holders. Place both of them in the same boat as was used for the glass substrates.

(c) When making adjustments in the HCl setting, a change of even 0.2 cms. is a significant change. It is possible to get good films by suitably adjusting the HCl. We have never had to readjust the N_2 or the O_2.

(d) The same procedure and settings are used for curing 1st and 2nd CdS films.

AD-A044 021 SYRACUSE UNIV N Y DEPT OF ELECTRICAL AND COMPUTER E--ETC F/G 9/5
TWO-DIMENSIONAL DIRECT ELECTRONIC FOURIER TRANSFORM (DEFT) DEVI--ETC(U)
JUN 77 S T KOWEL, P G KORNREICH, K W LOH DAAG53-76-C-0162
UNCLASSIFIED TR-77-5 NL

2 OF 2
AD
A044021

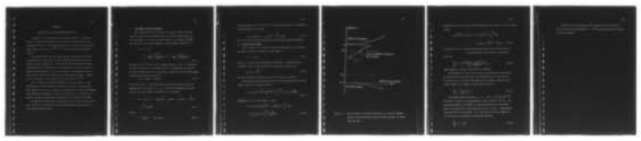

END
DATE
FILMED
10 -77
DDC

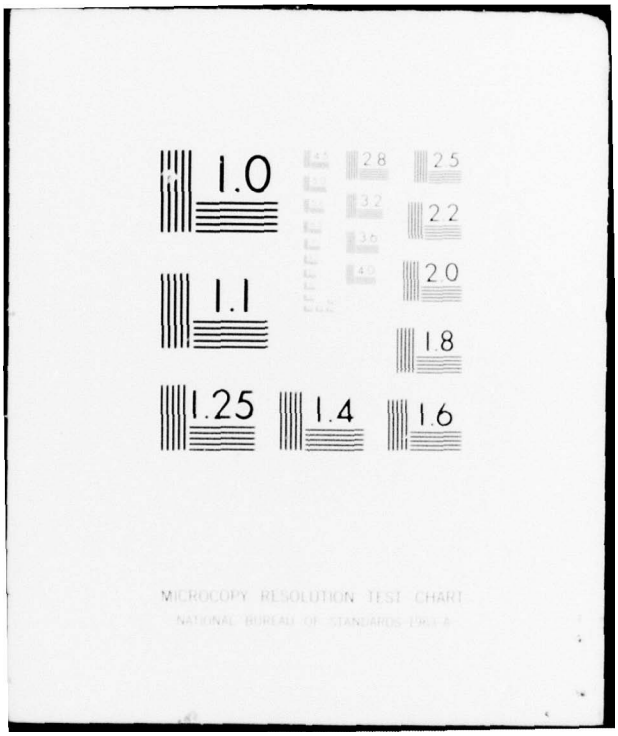
1.0
1.1
1.25
1.4
1.6
2.8
2.5
3.2
2.2
3.6
2.0
4.0
1.8
MICROCOPY RESOLUTION TEST CHART
NATIONAL BUREAU OF STANDARDS 1963-A

APPENDIX E

MECHANISM OF THE ELECTROPHOTOCONDUCTIVITY

A search of the literature has not been successful in yielding a theory of electrophotoconductivity which seems consistent with our experimental evidence. This appendix will serve to sketch a band-structure theory based on previous work[13, 14, 15] but with appropriate modifications.

We assume that the photoelectrons together with the electrons from ionized impurity states come to a quasi thermal equilibrium in the presence of steady illumination. This requires that the relaxation time τ_L associated with a redistribution of electrons due to light be much larger than the relaxation time τ_e of the electron redistribution due to a small energy shift of the conduction band and impurity states. Indeed τ_L is of the order of 1 ms while τ_e is of the order of 10^{-13} s.

In the following we calculate the effect of a small shift of the energy levels upon the number of conduction electrons. We assume that the conduction band edge is shifted by an amount equal to the Franz-Keldysh effect and that the impurity states in the energy gap are shifted by an amount of energy proportional to the shift of the conduction band edge.

We show that a small shift in energy has a large effect upon the number of conduction electrons due to the large impurity concentration in these photoconducting films.

E.1. THE NUMBER OF PHOTO ELECTRONS

Let us assume that in the presence of light the photo electrons come to a quasi-thermal equilbrium with an electron Fermi energy ε_{Fe}. The total number of free and trapped electrons, n_{co} and N_{t0}, including both electrons from ionized impurity states and photo electrons is

$$N = n_{co} + N_{to}$$

$$= c \int_{\varepsilon_c}^{\infty} \frac{(\varepsilon - \varepsilon_c)^{1/2} d\varepsilon}{\exp(\varepsilon - \varepsilon_{Fe})/kT + 1} + \int_0^{\varepsilon_c} \frac{g_t d\varepsilon}{\exp(\varepsilon - \varepsilon_{Fe})/kT + 1} \tag{E.1.1}$$

where $g_t(\varepsilon)$ is the density of the trapped electrons, and C is the density of states constant for a parabolic band.[1] Assuming that the conduction band is many kT above the quasi Fermi, energy, than one can approximate the Fermi distribution function by

$$f_1(\varepsilon) \simeq \exp-(\varepsilon - \varepsilon_{Fe})/kT \tag{E.1.2}$$

On the other hand, in the energy gap the Fermi distribution can be approximated by a unit step at $\varepsilon = \varepsilon_{Fe}$. With these assumptions the equation for the total number of electrons, (E.1.1) becomes

$$N = c\,[\exp-(\varepsilon_c - \varepsilon_{Fe})/kT)] \int_{\varepsilon_c}^{\infty} (\exp-(\varepsilon - \varepsilon_c)/kT)(\varepsilon - \varepsilon_c)^{\frac{1}{2}} d\varepsilon$$

$$+ \int_0^{\varepsilon_{Fe}} g_t(\varepsilon) d\varepsilon \tag{E.1.3}$$

Letting

$$u \equiv \frac{\varepsilon - \varepsilon_c}{kT}, \qquad du = \frac{1}{kT} d\varepsilon \tag{E.1.4}$$

and substituting (E.1.4) into (E.1.3) and integrating over u we obtain for the total number of electrons:

$$N = N_c \left[\exp -(\varepsilon_c - \varepsilon_{Fe})/kT + \int_0^{\varepsilon_{Fe}} g_t(\varepsilon)d\varepsilon \right. \tag{E.1.5}$$

Fig. E.1.1 shows the typical density of states versus energy distribution.

E.2 Electric Field Effect

In the presence of an electric field with components E_μ the conduction band is shifted in energy by a small amount $\Delta\varepsilon$

$$\Delta\varepsilon = \gamma_{\mu\nu} E_\mu E_\nu . \tag{E.2.1}$$

where $\gamma_{\mu\nu}$ is the tensor Franz-Keldysh coefficient. Assuming that the density of states in the energy gap is altered by an amount Δg_t,

$$\Delta g_t = \frac{\varepsilon}{\varepsilon_c} \Delta\varepsilon \frac{\partial g_t}{\partial \varepsilon} . \tag{E.2.2}$$

The Fermi energy is altered by the electric field by an amount a.

Substituting these changes into (E.1.5) where we assume that the total number of electrons remains constant

$$N = N_c \exp-\left(\frac{\varepsilon_c + \Delta\varepsilon - \varepsilon_{Fe} - a}{kT}\right) + \int_0^{\varepsilon_{Fe}+a} \left[g_t + \frac{\varepsilon}{\varepsilon_c} \Delta\varepsilon \frac{\partial g_t}{\partial \varepsilon}\right] d\varepsilon . \tag{E.2.3}$$

Expanding (E.2,3) to first order in $\Delta\varepsilon$ and a

$$N = N_c \exp-\left(\frac{\varepsilon_c - \varepsilon_{Fe}}{kT}\right) \left[1 - \frac{\Delta\varepsilon - a}{kT}\right] + \int_0^{\varepsilon_{Fe}} g_t d\varepsilon$$

$$+ g_t(\varepsilon_{Fe})a + \Delta\varepsilon \int_0^{\varepsilon_{Fe}} \frac{\varepsilon}{\varepsilon_c} \frac{\partial g_t}{\partial \varepsilon} d\varepsilon \tag{E.2.4}$$

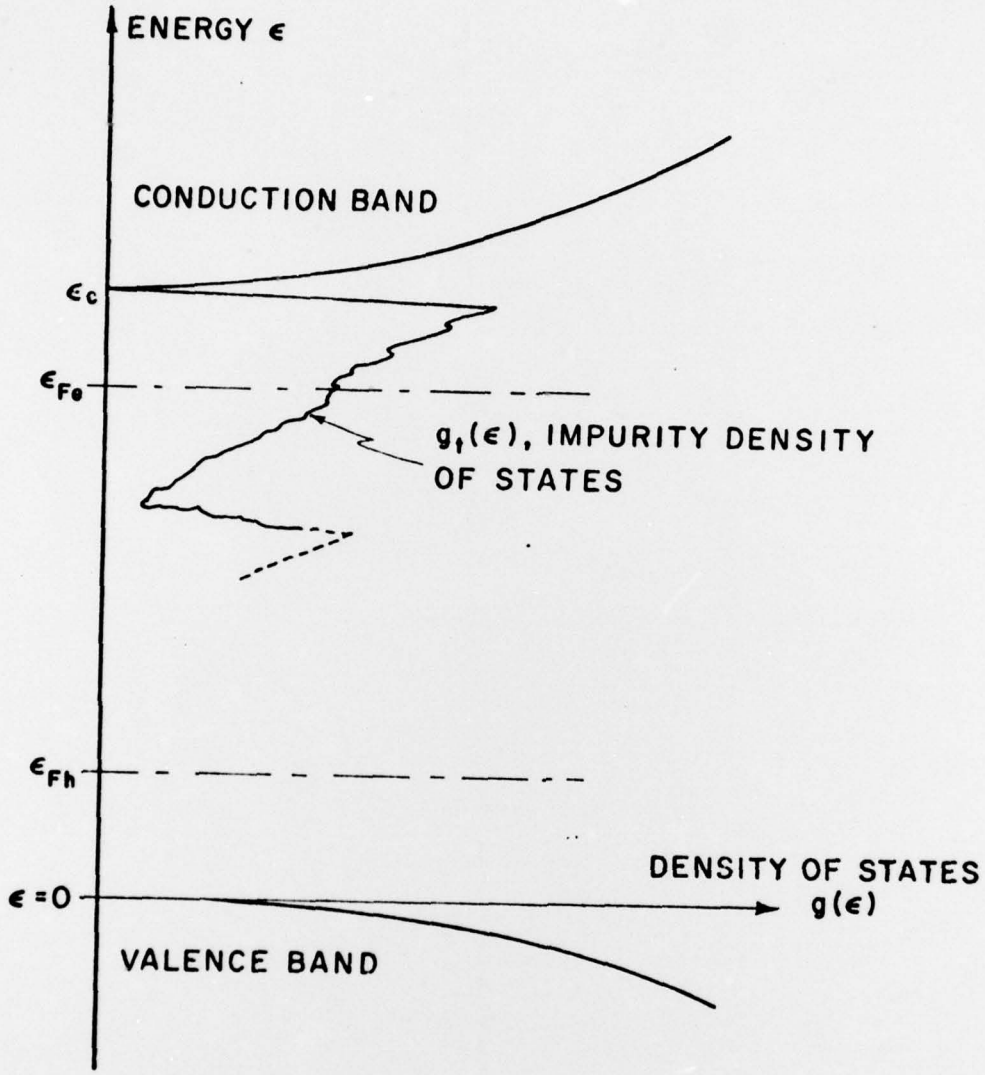

Fig. E.1.1. Typical density of states distribution of a CdS film showing impurity state distribution and quasi Fermi energies for electrons and holes.

Equating (E.1.1) and (E.2.4) and integrating the last term of (E.2.4) by parts yields,

$$n_{c0}\,\frac{\Delta\varepsilon - a}{kT} = g_t(\varepsilon_{Fe})a + \Delta\varepsilon\,\left[\frac{\varepsilon}{\varepsilon_c}\,g_t\right]_0^{\varepsilon_{Fe}} - \frac{\Delta\varepsilon}{\varepsilon_c}\int_0^{\varepsilon_{Fe}} g_t\,d\varepsilon$$

$$= g_t(\varepsilon_{Fe})\left[a + \frac{\varepsilon_{Fe}}{\varepsilon_c}\,\Delta\varepsilon\right] - \frac{\Delta\varepsilon}{\varepsilon_c}\,N_{t0}\,. \qquad (E.2.5)$$

Solving (E.2.5) for a and substituting the result into the first term of fractional change in the number of conduction electrons

$$\frac{\Delta n_c}{n_{c0}} = -\,\frac{\gamma_{\mu\nu}}{\varepsilon_c}\,\frac{g_t(\varepsilon_{Fe})[\varepsilon_c - \varepsilon_{Fe}] + N_{t0}}{n_{co} + g_t(\varepsilon_{Fe})kT}\,E_\mu E_\nu\,. \qquad (E.2.6)$$

where summation over like Greek indices is implied.

The numerator is of the order of the total number N_T of trap states per unit volume in the energy gap. The denominator is of the order of the number n_{c0} of conduction electrons per unit volume. Thus the fractional change of the number of conduction electrons is

$$\frac{\Delta n_c}{n_{c0}} \approx -\,\frac{N_T}{n_{c0}}\,\frac{\gamma_{\mu\nu}}{\varepsilon_c}\,E_\mu E_\nu\,. \qquad (E.2.7)$$

The Franz-Keldysh coefficient $\gamma_{\mu\nu}$ is $\approx -1.62 \cdot 10^{-16}\ eVm^2/V^2$ [15]. The electric fields in our experiment are small, typically 10^4 V/m. The percentage change in the number of conduction electrons in our experiments is typically 20%! The energy gap of CdS is 2.42 eV. Substituting this data into (E.2.6) we obtain for the ratio of the total number N_T of trap states to the number of conduction electrons

$$\frac{N_T}{n_{c0}} \approx 3 \cdot 10^7. \qquad (E.2.8)$$

Since there are approximately 10^{18} conduction electrons per m^3 these films contain approximately $3 \cdot 10^{25}$ impurity states per m^3 which is quite reasonable.